Research Square

Preprints are preliminary reports that have not undergone peer review.
They should not be considered conclusive, used to inform clinical practice,
or referenced by the media as validated information.

Discovery, Synthesis and Structural Insights into a New Family of Positive Allosteric Modulators for MRGPRX1

Lauri Louhivuori

lauri.louhivuori@orionpharma.com

Orion Pharma https://orcid.org/0000-0001-8649-781X

Ainoleena Turku-Metsänen

Orion https://orcid.org/0000-0003-0959-7221

Alexander Ulrich

Nuvisan ICB GmbH https://orcid.org/0000-0003-4255-4856

Yansong Wang

Nuvisan ICB GmbH

Muriel Joubert

Orion Pharma

Cecilia Jungarå

Orion Pharma

Maija Ivaska

Orion Pharma

Hugh Chapman

Orion Pharma

Andrii Domanskyi

Orion Pharma https://orcid.org/0000-0002-4755-5981

Katrin Nowak-Reppel

Nuvisan ICB GmbH

Vera Puetter

Nuvisan ICB GmbH

Duy Nguyen

Nuvisan ICB GmbH

Holger Monenschein

Nuvisan

Article

Keywords:

Posted Date: June 4th, 2026

DOI: https://doi.org/10.21203/rs.3.rs-9654557/v1

License: This work is licensed under a Creative Commons Attribution 4.0 International License.
Read Full License

Additional Declarations: There is **NO** Competing Interest.

Discovery, Synthesis and Structural Insights into a New Family of Positive Allosteric Modulators for MRGPRX1

Ainoleena Turku-Metsänen[1#], Alexander K. C. Ulrich[2], Yansong Wang[2], Muriel Joubert[1], Cecilia Jungarå[1], Maija Ivaska[1], Hugh Chapman[1], Andrii Domanskyi[1], Katrin Nowak-Reppel[2], Vera Puetter[2], Duy Nguyen[2], Holger Monenschein[2], Lauri M. Louhivuori[1#]

[1] R&D, Orion Pharma, Finland

[2] Nuvisan ICB GmbH, Berlin 13353, Germany.

to whom correspondences should be addressed.

Abstract

The human Mas-related G protein–coupled receptor X1 (MRGPRX1) has emerged as a promising non-opioid analgesic target owing to its selective expression in primary nociceptive sensory neurons. While full agonism, especially in peripheral nervous system, may induce itch sensation, positive allosteric modulators (PAMs) enhance receptor signalling in a ligand-dependent manner, providing physiological selectivity over orthosteric agonists. Here, we report the discovery of novel PAMs of MRGPRX1. These compounds were identified through a structure-based virtual screening campaign followed by iterative compound optimization. Target engagement of the compounds was confirmed, and their modes of action were delineated using a novel surface plasmon resonance (SPR) assay that discriminates between distinct modes of action (antagonist, agonist and PAM), alongside cellular assays confirming positive allosteric modulation of MRGPRX1. In parallel, we established a robust protein production and cryo-EM workflow, enabling high-resolution cryo-EM structures of MRGPRX1 in complex with Gqα-Gβ-Gγ heterotrimer and bound to the MRGPRX1 ligand BAM8-22 together with the discovered PAMs. Collectively, these findings advance mechanistic insight into positive allosteric modulation of MRGPRX1 and provide a basis for the rational design of targeted therapeutics for chronic pain and pruritus.

Introduction

G protein-coupled receptors (GPCRs) represent the largest and most diverse family of membrane proteins, playing pivotal roles in cellular signaling and serving as key therapeutic targets across a wide range of diseases [1]. Their ability to modulate multiple ion channels simultaneously offers a strategic advantage in drug development, particularly for complex conditions such as chronic pain and pruritus.

Among the GPCR subfamilies, the primate specific Mas-related G protein-coupled receptors of subfamily X (MRGPRX) have emerged as mediators of non-histaminergic itch sensation, inflammation, and pain. In humans, four MRGPRX members (MRGPRX1-4) have been identified, with MRGPRX1 attracting particular attention due to its intriguing dual functionality in pain and pruritus and its predominant expression in dorsal root ganglia and trigeminal ganglia root neurons [2]. MRGPRX1 is classified as an orphan GPCR. Endogenous enkephalin fragments, such as those derived from pro-enkephalin A peptides, have been shown to activate MRGPRX1 with BAM8-22 peptide the most potent of the series [3]. Peripheral injection of BAM8-22 induces itch [4], while intrathecal application in humanized mouse models induces analgesic effects, suggesting a context-dependent role in sensory modulation [5,6].

Notably, positive allosteric modulators (PAMs) have been found to enhance MRGPRX1 activation by BAM8-22, with coupling to different Gα subunits (Gαq and Gαi) influencing downstream effects [7]. PAM compounds like ML382 (later referred as **1**) [8] exemplify the pharmacological complexity of targeting MRGPRX1, where modulation of voltage-gated calcium channels (VGCCs), TRPA1 [9] and TRPV1 receptors [10], and tetrodotoxin-resistant sodium channels [11] have been reported to contribute to pain inhibition, while itch is mediated through non-histaminergic pathways [2]. Despite its therapeutic promise, the development of selective modulators for

MRGPRX1 remains challenging. Additionally, PAMs with minimal intrinsic agonistic activity are particularly difficult to optimize. One reason for this might be that compounds with this mode of action bring additional complexity to the assay design.

In this study, we report the discovery of novel PAMs of MRGPRX1. These compounds were identified through a structure-based virtual screening campaign followed by iterative compound optimization. We demonstrate on-target binding of the best compounds and their mode of action by biophysical measurement in a novel surface plasmon resonance (SPR) assay, which can differentiate different modes of action. Positive allosteric modulation was confirmed in a cellular assay where the shift of endogenous agonist BAM8-22 activity was measured. Furthermore, we present cryo-electron microscopy (cryo-EM) structures of the MRGPRX1 receptor in complex with the Gqα-Gβ-Gγ heterotrimer, bound to the peptide ligand BAM8-22 and two of the newly identified PAMs. Collectively, these findings provide deeper understanding of positive allosteric modulation of MRGPRX1 and offer a foundation for the rational design of targeted therapeutics aimed at treating chronic pain and pruritus.

Results

Virtual screening identified positive allosteric modulators of MRGPRX1

At the outset of this study, structural information on the MRGPRX1 receptor was limited, with only a single positive allosteric modulator-bound cryo-EM structure available [12]. Intriguingly, the structure indicates that PAM **1** (**Supplementary Information Figure S1**) is bound to the orthosteric binding site of the MRGPRX1 between the peptide agonist BAM8-22 and the receptor. Visual inspection and WaterMap analysis (Schrödinger Suite 2022-4) suggested that water

molecules play a critical role in the binding of compound **1** even though they were not visible in the original structure. Incorporating these water molecules into docking-based virtual screening was hypothesized to enhance predictive accuracy.

To optimize the positioning of water molecules within the binding site, a 100 ns molecular dynamics (MD) simulation was performed. The G-protein component of the receptor complex was modeled as miniGq, using the sequence reported by Nehme et al. [13]. Every 10th trajectory frame was extracted, excluding the initial 50 ns to allow for system equilibration. We selected frames for further analysis based on two criteria: (1) **1** exhibited the desired interaction pattern with the receptor, and (2) a water molecule was located within 2.5 Å of the sulfonamide nitrogen atom of **1**.

Docking grids were constructed based on the selected frames and evaluated for their ability to discriminate active compounds (Schrödinger Suite 2023-1). Thirteen known actives [8,14] and 364 property-matched decoys from the screening library were used to assess grid performance. The best-performing grid was selected for virtual screening.

Virtual screening was conducted using pre-filtered Enamine REAL database and HASTEN software [15] in four iterative rounds. After post-processing, we purchased 269 compounds from the Enamine REAL database for experimental validation.

Activities of the 269 virtual hit compounds were assessed in functional PAM/agonist assays. BAM8-22 was used as the ligand to activate human MRGPRX1 with both calcium (via FLIPR measurement) and IP3 activity (via measurement of downstream IP1/IP-One utilizing TR-FRET) assessed. Using the parental HEK293 cell line, it was modified to stably expresses the human MRGPRX1 receptor protein (hereinafter called HEK-X1 cells). BAM8-22 induced a clear response-curve in HEK-X1 cells with an EC_{50} of 3.73 nM (n=16, N=4) in calcium FLIPR and

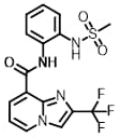
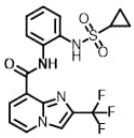
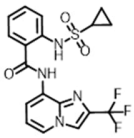
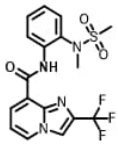
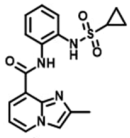
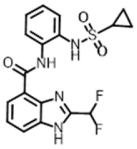
95.3 nM (n=12, N=3) in TR-FRET assays, whereas no responses were recorded in the naive HEK-293 cells lacking MRGPRX1. The PAM activity of the compounds was also detected in the calcium FLIPR and the IP-One TR-FRET PAM assays. A double addition protocol was employed for calcium FLIPR assay to characterize the PAM properties of the compounds. The cells were treated with the compounds to assess agonistic assay followed by co-treatment with a low fixed concentration of BAM8-22, equivalent to EC_{10}-EC_{30} of BAM8-22, to assess the positive modulation of the tested compounds. Furthermore, control HEK293 cells with no MRGPRX1 receptor were utilized for potential off-target effects. Compound **1** displayed in the calcium FLIPR assay PAM activity with EC_{50} value of 0.99 µM (n=16, N=4) and agonistic activity with EC_{50} value of 4.0 µM (n=16, N=4), respectively. In the IP-One TR-FRET assay, **1** EC_{50} was 6.2 µM (n=4, N=2) with agonistic activity at 12.2 µM (n=4, N=2). Compound **1** did not show activity in naive HEK293 cells. Single concentration (30 µM) screening of the 269 compounds in calcium FLIPR assay resulted in 15 initial hits, where PAM and agonistic activities were used as filtering criteria. Of the 15 compounds, 67% of compounds displayed no clear concentration-dependent responses, while 20% of compounds were agonistic, and 13% of compounds displayed a more pronounced PAM activity. Among the initial hits, compound **2** was selected for further studies due to its promising PAM activity without any agonistic activity (>25 µM in IP-One TR-FRET assay) combined with favorable lead-like properties.

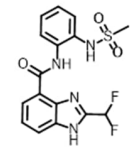
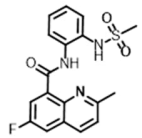
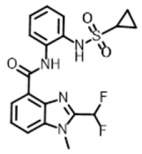
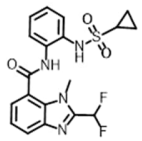
SAR around compound 2

Compound **2** displayed activity in FLIPR PAM assay with EC_{50} at 0.94 µM (**Table 1**). The imidazopyridine core and the northern aryl moiety of **2** was connected by an amide bridge in a reverse way as compared to **1**, dubbed as “reversed amide”. First analogs of **2** included the

cyclopropyl derivative **3** with slightly better activity with EC_{50} at 0.68 µM. Interestingly, the same cyclopropyl derivative combined with the amide as found in **1**, compound **4**, was notably less active, highlighting the importance of the reverse amide bridge. *N*-methylation of the sulfonamide moiety leading to **5** with EC_{50} at 1.09 µM, without compromising activity as compared to **2**, suggesting this N-H bond of the sulfonamide moiety did not contribute to the affinity to MRGPRX1. Replacement of the trifluoromethyl group by a less lipophilic methyl group resulted in slightly reduced activity with EC_{50} at 1.37 µM for compound **6**.

Table 1. Compound 2 SAR.

Compound ID	Structure	FLIPR PAM qAC50 (µM)	FLIPR Ago qAC50 (µM)	Fold change FLIPR (Ago/ PAM)	TR-FRET PAM qAC50 (µM)	TR-FRET Ago qAC50 (µM)	Fold change TR-FRET (Ago/ PAM)
2		**0.94[a]**	**19.2[a]**	**20.4**	**1.65[a]**	**> 25[a]**	**> 15**
3		**0.68[a]**	**19.2[a]**	**28.2**	**0.75[a]**	**> 25[a]**	**> 33**
4		**14.4[b]**	**19.2[b]**	**1.3**	**25[a]**	**> 25[b]**	**> 1**
5		**1.09[a]**	**6.4[a]**	**5.9**	**0.89[a]**	**> 25[a]**	**> 28**
6		**1.37[a]**	**19.2[a]**	**14.0**	**1.95[a]**	**> 25[a]**	**> 13**
7		**0.14[c]**	**11.6[c]**	**83.5**	**0.11[a]**	**> 25[a]**	**> 227**

8		**0.19[a]**	**3.92[a]**	**20.6**	**0.31[a]**	**> 25[a]**	**> 81**
9		**0.13[c]**	**2.14[c]**	**16.5**	**0.13[a]**	**1.76[a]**	**13.5**
10		**0.36[a]**	**7.77[a]**	**21.6**	**0.08[a]**	**14.3[a]**	**178.8**
11		**14.4[a]**	**19.2[a]**	**1.3**	**16.1[a]**	**> 25[a]**	**> 1.5**

[a]n=4, N=2
[b]n=2, N=1
[c]n=6, N=3

As compound **3** displayed reasonable potency we set out to test its ability to modulate voltage gated calcium channel activity (VGCC) via MRGPRX1, as this is one of the endpoints for analgesic efficacy in sensory neurons. Manual patch clamp studies on rat DRG neurons overexpressing the human MRGPRX1 receptor in vitro were run. In line with previous reports [5,16], neuronal high voltage activated (HVA) calcium current (I_{Ca}), in contrast to the markedly smaller low voltage activated (LVA) I_{Ca}, was robustly inhibited by MRGPRX1 activation. As seen in **Figure 1A-C**, overexpression of human MRGPRX1 resulted in a significant inhibition of the peak HVA I_{Ca} amplitude by 5 µM BAM8-22 (52.9 ± 2.6 %, n = 14 vs only GFP expressing: 3.5 ± 1.0 %, n = 9; P <0.001). This maximal inhibition with 5 µM BAM8-22 was then used to assess the agonism and PAM effect of **3**. Compound **3**, at 1 µM, potentiated the minor inhibitory effect on HVA I_{Ca} of a low concentration of BAM8-22, the relative inhibition compared to 5 µM BAM8-22 increasing from 3 % to 50 % with the combination (**Figure 1E-F**). Compound **3** by itself produced little inhibition (**Figure 1D**).

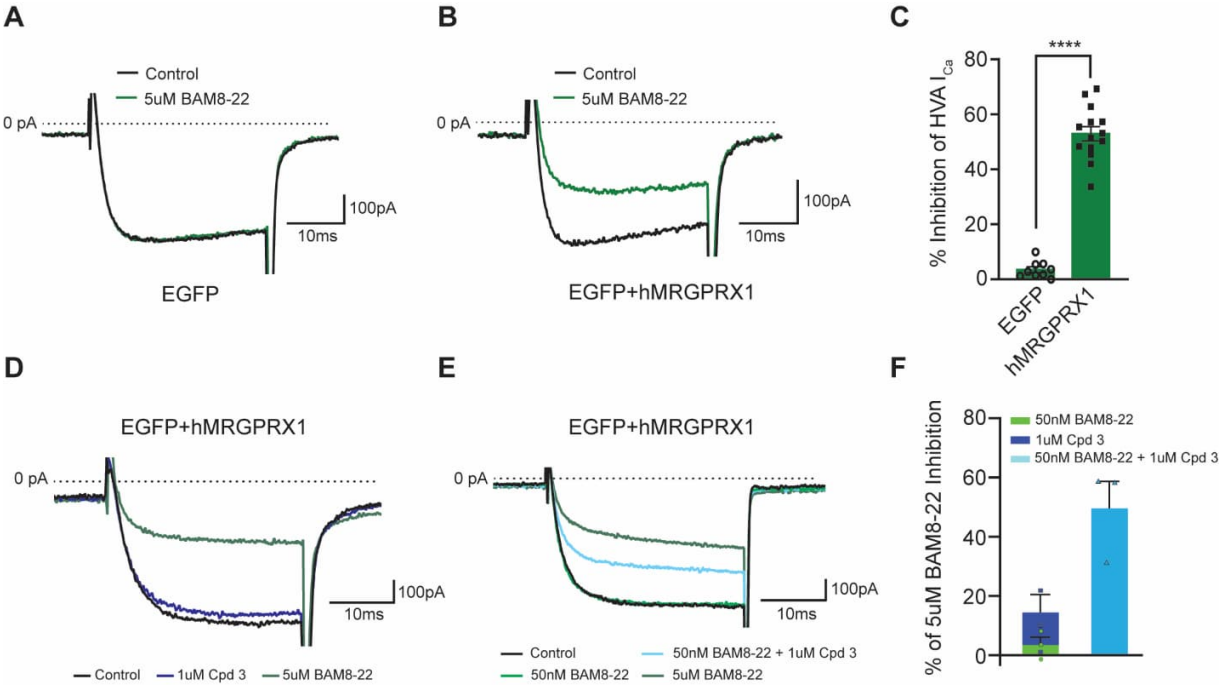


Figure 1: Effect of BAM8-22 and compound 3 on high voltage activated (HVA) calcium current (I_{Ca}). Whole-cell patch clamp recordings of the HVA I_{Ca} of rat DRG neurons transduced with EGFP (**A**) or EGFP + hMRGPRX1 (**B**). The HVA I_{Ca} was evoked by a 30 ms depolarization to -10 mV from -60 mV. **C**, Percentage inhibition by 5 µM BAM8-22 of the HVA I_{Ca} of rat DRG neurons transduced with GFP (n = 9, each dot represents a distinct measurement, mean and standard error of mean plotted) or GFP + hMRGPRX1 (n = 14, each dot represents a distinct measurement, mean and standard error of mean plotted). Statistical difference was assessed using two-sided unpaired students t-test (**** p<0.0001). Normality was assessed using the Shapiro–Wilk test (W = 0.91, p = 0.3, n=9 W=0.98, p=0.98, n=14), indicating no significant deviation from normality, therefore comparisons were performed using a parametric t-test. **D**, The effect of 1 µM compound **3** and 5 µM BAM8-22 on the HVA I_{Ca} of a hMRGPRX1 transduced DRG neuron. **E**, The effect 50 nM BAM8-22 alone and in combination with 1 µM compound **3** on the HVA I_{Ca} of a hMRGPRX1 transduced DRG neuron. **F**, Relative inhibition of HVA I_{Ca} by 50 nM BAM8-22 and 1 µM compound **3** separately and combined (n = 3 in each case. Each dot represents a distinct measurement. Mean and standard error of mean plotted).

We hypothesized that the reverse amide bond found in **3** enabled the formation of an intramolecular hydrogen bond between the amide -N-H and the nitrogen in the imidazopyridine core, which should contribute to the stabilization of a conformation required for affinity to the MRGPRX1. If this hypothesis is true, we should be able to use this design principle to expand to other chemical series.

In order to probe our hypothesis, we synthesized difluoromethyl substituted benzimidazole derivatives **7** and **8** as well as quinoline derivatives such as **9**. All 3 compounds were active (with EC_{50} 0.14 μM, 0.19 μM and 0.13 μM, respectively; **Table 1**). In the benzimidazole series, *N*1-methylation resulted in **10** (0.36 μM) without compromising the potency as compared to **7** (0.14 μM), which contrasts with the *N*3-methylated derivative **11** (14.4 μM).

The identified PAMs bind to MRGPRX1 in presence of BAM8-22

To demonstrate direct target engagement of the novel allosteric modulators, SPR was employed. For binding of agonists to occur, GPCRs must undergo a conformational change into an active protein conformation. As this conformational change may not be possible under conventional SPR conditions, we expressed and purified biotinylated MRGPRX1 both by itself and in complex with an engineered Gqα (miniG) protein. In the complex, MRGPRX1 would be locked in an active conformation and would not need to undergo conformational changes to allow binding of agonists. The purified MRGPRX1 and MRGPRX1/Gqα samples were captured via biotin on a streptavidin sensor chip. To demonstrate that the purified protein samples are pharmacologically active but in different conformational states, interactions with well-characterized ligands were examined (**12** as antagonist, BAM8-22 as agonist, and **13** as PAM were used; for reference compound structures, see **Supplementary Information Figure S1**). The SPR experiments showed concentration-

dependent binding of the antagonist **12** to both MRGPRX1 alone and the MRGPRX1/Gqα complex (**Figure 2 A1 and B1**). The agonist BAM8-22 bound only to the MRGPRX1/Gqα complex, not to MRGPRX1 alone (**Figure 2 A2 and B2**). This indicates that the immobilized MRGPRX1 samples indeed adopt different conformations, with the complex being in an active conformation, consistent with published cryo-EM structures[7,12]. Binding of the positive allosteric modulator **13** to the MRGPRX1/Gqα complex was observed only in the presence of BAM8-22 (**Figure 2 A3-4 and B3-4**), which is characteristic PAM-like behavior. This set-up was used to investigate the mode of action (MoA) of our compounds.

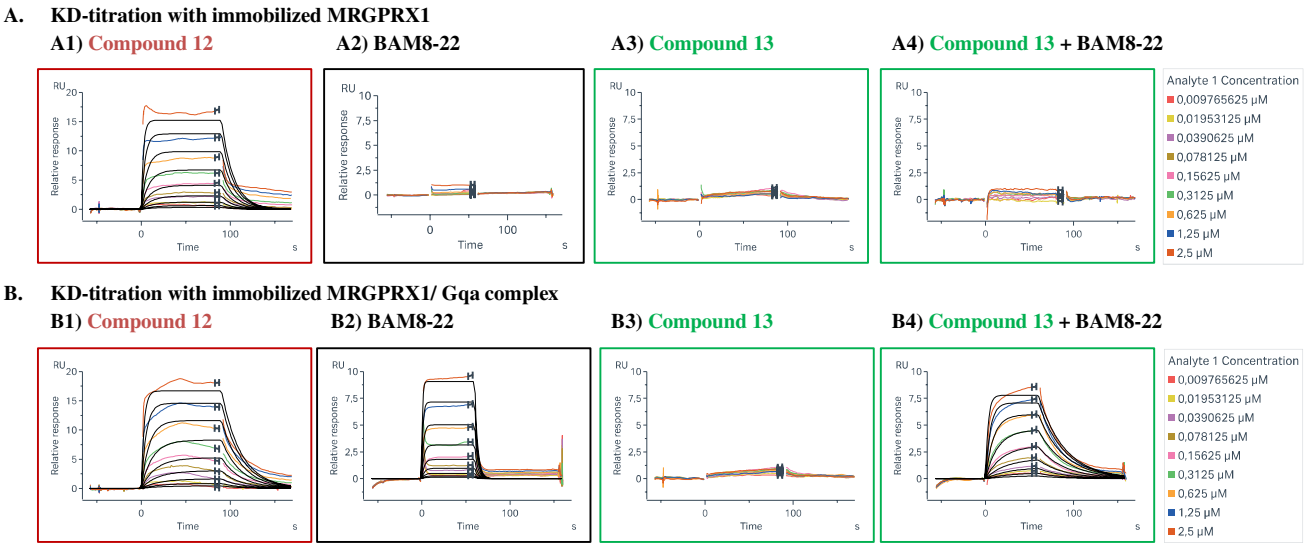


Figure 2: SPR sonograms of compound binding to MRGPRX1 (A) and MGPRX1/Gqa complex (B). Concentration-dependent binding curves of **1)** compound **12** (antagonist), **2)** BAM8-22, **3)** PAM and **4)** BAM8-22 + PAM (19, 29, 78, 156, 312, 625, 1250 and 2500 nM compound concentration) to immobilized MRGPRX1 **(A 1-4)**, MRGPRX1 /Gqa complex **(B 1-4)**. In experiment 4 the running buffer contained 5µM BAM-8-22. Experiments were performed in triplicates.

Nine compounds were tested in SPR for binding to MRGPRX1 and MRGPRX1/Gqα in the absence and presence of BAM8-22 in the running buffer (**Table 2**). For seven compounds, binding

to the MRGPRX1/Gqα complex in the presence of BAM8-22 was confirmed, with dissociation constants (KDs) in the range 90 nM – 5 µM. None of the tested compounds bound to MRGPRX1 alone or to MRGPRX1/Gqα in the absence of BAM8-22. These observations suggest that these compounds are PAMs, in agreement with cell-based assay results. Based on all these results combined, **8** and **9** were selected for further studies (**Figure 3**).

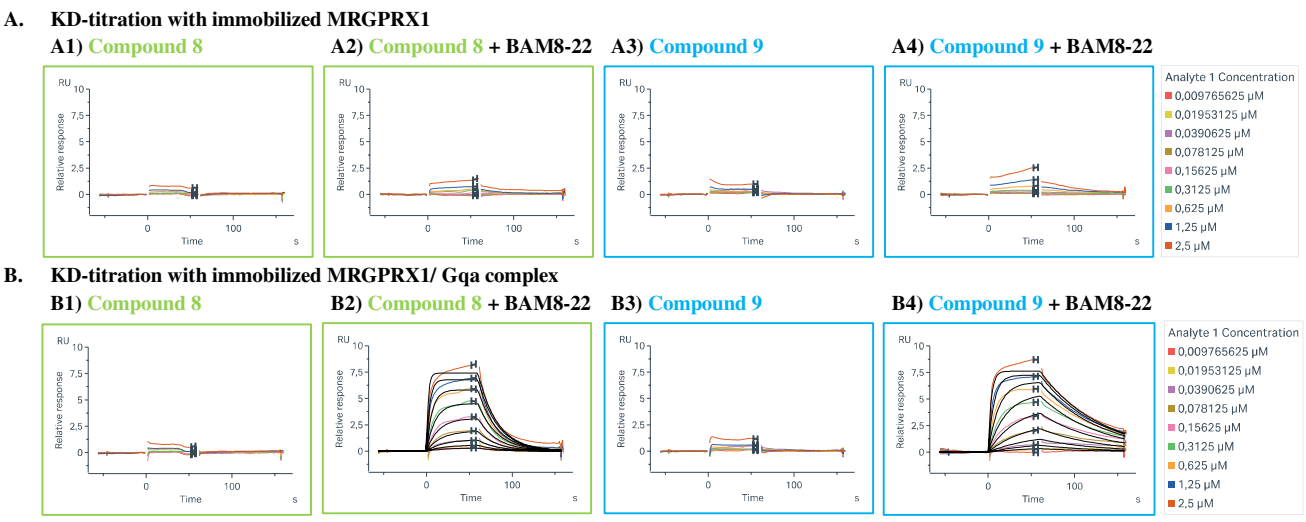


Figure 3: SPR sonograms of compound binding to MRGPRX1 (A) and MGPRX1/Gqa complex (B). Concentration-dependent binding curves of **1)** compound **8**, **2)** compound **8** + 5µ BAM8-22, **3)** compound **9** and **4)** compound **9** + 5µM BAM8-22 (19, 29, 78, 156, 312, 625, 1250 and 2500 nM **8** and **9** concentration) to immobilized MRGPRX1 **(A 1-4)**, MRGPRX1/Gqa complex **(B 1-4)**. In experiments 2 and 4 the running buffer contained 5µM BAM-8-22. Experiments were performed in triplicates.

Table 2: KD values determined by SPR

Compound	KD (µM) mean	kd (1/s) mean	ka (1/Ms) mean	Rmax (RU) mean	SE(ka) (1/Ms) mean	SE(kd) (1/s) mean	SE(Rmax) (RU) mean	Kinetics Chi² (RU^2) mean	FLIPR PAM qAC50 (µM)
3	0.43	6.07e+04	2.06e-02	8.3	8.57e+02	1.05e+02	0.04	0.52	0.68
4	> 5	ND	ND	ND	ND	ND	ND	ND	14.4
5	0.82	5.49e+04	3.63e-02	9.9	6.93e+02	4.91e+01	0.05	0.54	1.09
6	1.88	1.32e+05	1.50e-01	12.6	1.21e+03	2.31e+02	0.11	0.17	1.37
7	0.44	1.13e+05	4.33e-02	11.6	7.94e+02	1.42e+02	0.04	0.61	0.14
8	0.24	2.23e+05	4.97e-02	10.4	3.16e+03	1.89e+02	0.03	0.95	0.19
9	0.12	1.66e+05	1.91e-02	10.1	1.99e+03	2.50e+02	0.03	0.94	0.13
10	0.18	2.44e-02	1.40e+05	2.6	1.70e+03	1.66e-04	0.01	0.07	0.36
11	> 5	ND	ND	ND	ND	ND	ND	ND	14.4
13	0.31	1.15e+05	3.44e-02	7.6	3.01e-04	1.89e+03	0.04	0.08	0.04

ND, not determined

Compounds 8 and 9 potentiate the effect of BAM8-22 with no effect on E_{max}

The PAM activity of the compounds were detected in the FLIPR and TR-FRET PAM assays in which a fixed low BAM8-22 concentration was applied in combination with the compounds. A higher potency in these PAM assays compared to simple agonist assays, in addition to the SPR results, already suggested a positive allosteric mode-of-action. To assess the range the identified PAMs can potentiate the MRGPRX1 activation by the orthosteric agonist BAM8-22 and whether they are able to modulate E_{max} in concordance with EC_{50} shifts, BAM8-22 shift assays in the FLIPR assay setup were performed. Concentration response curves (CRCs) of BAM8-22 were determined alone or with simultaneous application of increasing concentrations of the compound. Positive allosteric modulators would show co-operativity, i.e. shift the BAM8-22 CRC to higher potencies depending on the applied concentration, with no change seen in E_{max} values.

In our FLIPR BAM8-22 shift assays the CRC of BAM8-22 was left-shifted to higher potencies with increasing concentrations of **8** or **9** (**Figure 4**). While a BAM8-22 concentration of 0.1 nM alone did not stimulate MRGPRX1, a simultaneous application of 1.05 µM **8** or **9** showed already 50% activation. This demonstrates the concentration-dependent potentiation of the stimulation by the agonist BAM8-22. Additionally, BAM8-22 with addition of either **8** or **9** did not show any change of E_{max} values in comparison to CRC of BAM8-22 alone.

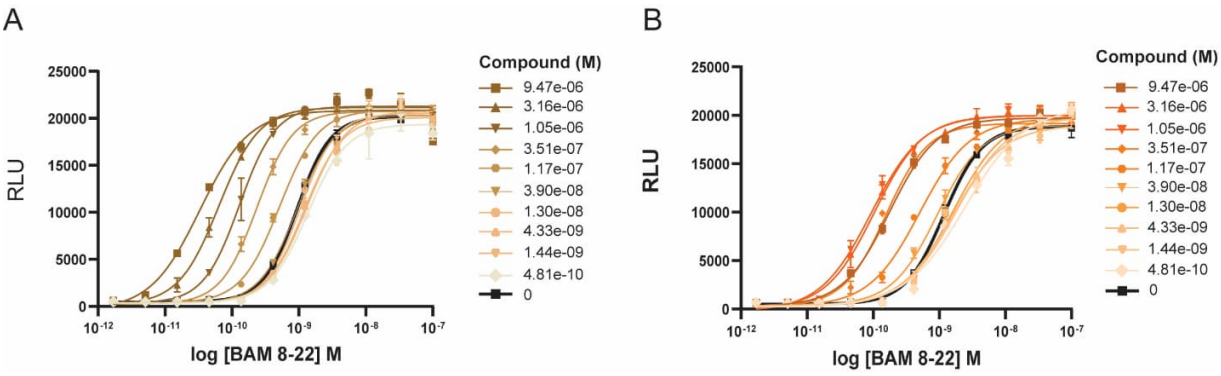


Figure 4: BAM8-22 shift assay of compounds 8 (A) and 9 (B). Concentration-response curve of an 11-point dilution series of BAM8-22 alone (black curve) with addition of 11 different concentrations of **(A)** compound **8** (brown shaded curves) (n=2, N=1) and **(B)** compound **9** (orange shaded curves) (n=2, N=1).

Cryo-EM structures of MRGPRX1-Gqα-Gβ-Gγ-scFv16–BAM8-22–PAM complexes

For structural studies, the MRGPRX1-Gqα-Gβ-Gγ complex was assembled by co-expression of the GPCR with G-protein constructs and purified by M2 Flag affinity purification. After incubation with the G-protein complex stabilizing antibody fragment scFv16 [17] the complex was subjected to a final size exclusion chromatography purification.

The cryo-EM structure of MRGPRX1-Gqα-Gβ-Gγ-scFv16 in complex with BAM8-22 and PAM **9** was determined at 2.33 Å (global refined map **Figure 5a, Supplementary Information Table S1, Supplementary Information Figure S2**). The map quality and local resolution of the PAM binding region was improved by local refinement with a focused mask covering the receptor chain and BAM8-22, resulting in a local refined map at 2.63 Å and a local resolution of the ligand density of 2.4-2.6 Å (**Figure 5b, Supplementary Information Table S1, Supplementary Information Figure S2**). The cryo-EM structure of MRGPRX1-Gqα-Gβ-Gγ-scFv16 in complex with BAM8-22 and PAM **8** was determined at 2.63 Å (global refined map **Figure 5c, Supplementary Information Table S1, Supplementary Information Figure S3**). The map quality and local resolution of the PAM binding region was improved by local refinement with a focused mask covering the receptor chain and BAM8-22, resulting in a local refined map at 2.87 Å and a local resolution of the ligand density of 2.6-2.7 Å (**Figure 5d, Supplementary Information Table S1, Supplementary Information Figure S3**). The local refinement especially improved the map quality for BAM8-22, the PAM, and the extracellular side of MRGPRX1 (**Supplementary Information Figure S4**), a region that – without local refinement – is often relatively poorly resolved in GPCR cryo-EM structures [7,12,18-20].

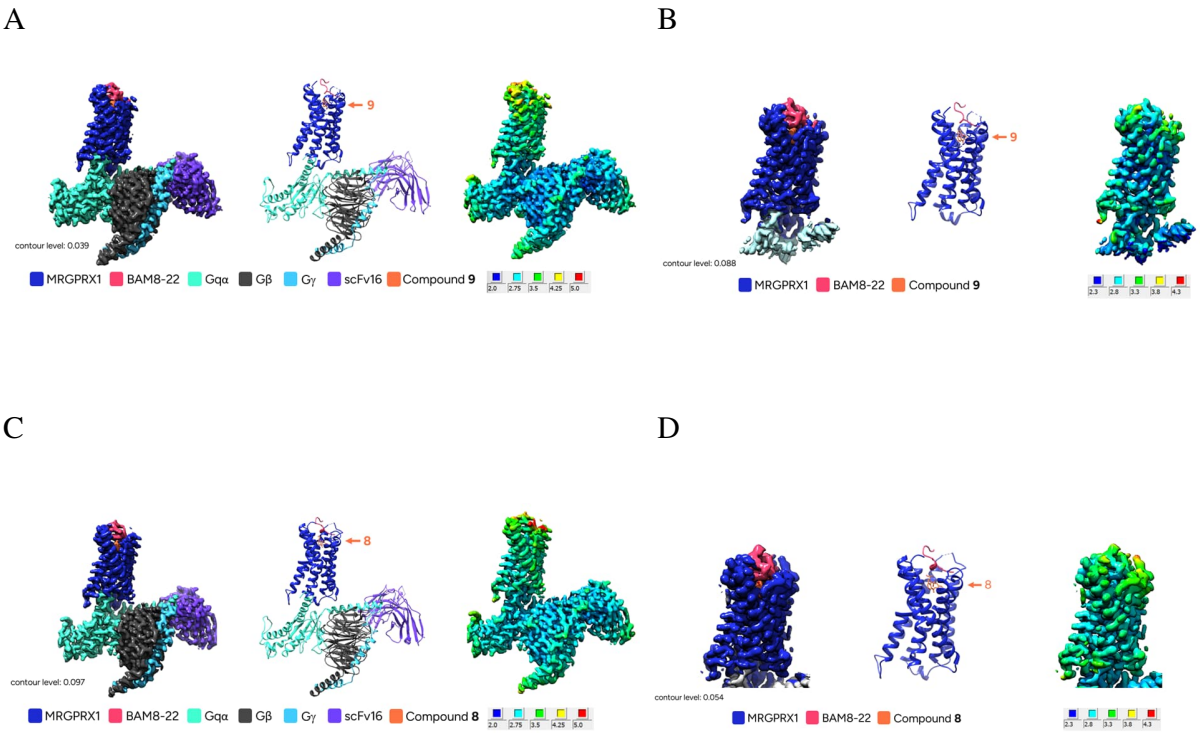


Figure 5: MRGPRX1-9 and MRGPRX1-8 cryo-EM structures.

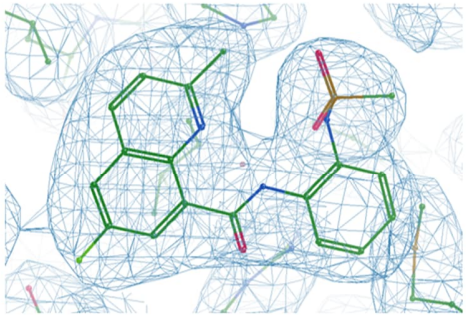
Depicted are the cryo-EM density map, cartoon representation, and local resolution map for **(A)** global refined MRGPRX1-**9** structure, **(B)** local refined MRGPRX1-**9** structure, **(C)** global refined MRGPRX1-**8** structure, **(D)** local refined MRGPRX1-**8** structure.

Binding modes of PAMs 8 and 9

Compounds **9** (**Figure 6a and 6b**) and **8** (**Figure 6c and 6d**) both bind to an allosteric pocket at the extracellular side of MRGPRX1, below the orthosteric agonist peptide BAM8-22. The binding modes of **9** and **8** are similar to the binding mode of PAM **1** that binds to the same pocket [12]. Compounds **9** and **8** both form hydrogen bonds via the peptide bond carbonyl oxygen to Arg79 (TM2) and via a sulfonamide oxygen to His254 (TM7). Both compounds form an intramolecular hydrogen bond between the amide NH group and the quinoline nitrogen (**9**) or the benzimidazole

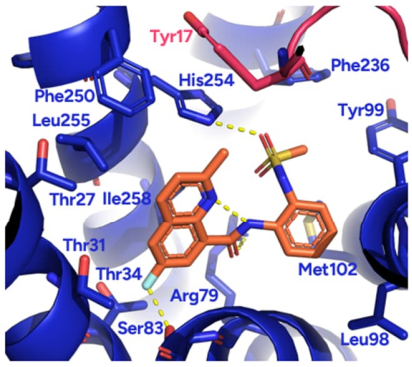
nitrogen (**8**), providing confirmation of our design principle. In addition, **9** forms a hydrogen bond via the quinoline fluorine to the hydroxyl group of Ser83 (TM2), while **8** forms a hydrogen bond via a difluoromethyl fluorine to the hydroxyl group of Tyr82 (TM2). In the cryo-EM map of **8**, we also observe a water molecule in hydrogen bond distance to the benzimidazole NH group, but we did not observe other water molecules or protein residues in vicinity of this water molecule. Compounds **9** and **8** are engaged in hydrophobic interactions with MRGPRX1 residues Thr31, Tyr82 (π-stacking), Leu98, Tyr99, Met102, Phe236, Phe250, Leu255, and Ile258, as well as with Tyr17 of BAM8-22. In addition, **9** is engaged in a hydrophobic interaction between its quinoline fluorine and the aliphatic portion of Thr34.

A



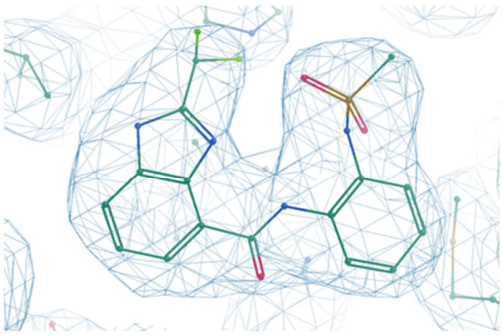
Ligand density
contour level: 0.065 (rmsd 4.5)

B



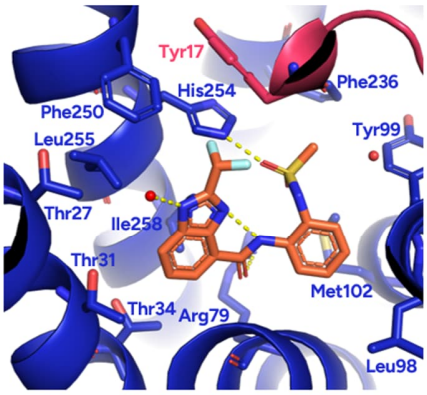
Ligand binding site
MRGPRX1 BAM8-22 Compound **9**

C



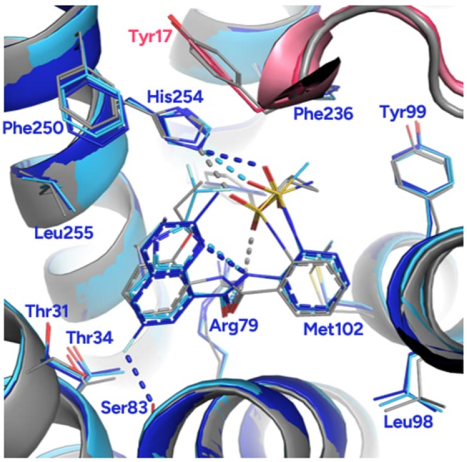
Ligand density
contour level: 0.099 (rmsd 4.5)

D



Ligand binding site
MRGPRX1 BAM8-22 Compound **8**

E



Ligand binding site
MRGPRX1 + Compound **9** BAM8-22
MRGPRX1 + Compound **8** BAM8-22
MRGPRX1 + Compound **1** + BAM8-22

Figure 6: Ligand binding sites of 9 and 8.

A, Cryo-EM density around **9** contoured at 4.5 rmsd, **B**, **9** binding site, **9** and residues interacting with **9** are shown as sticks. Tyr82 is not shown for clarity. Hydrogen bonds are shown as dashed lines. **C**, Cryo-EM density around **8** contoured at 4.5 rmsd, **D**, **8** binding site, **8** and residues interacting with **8** are shown as sticks. Tyr82 is not shown for clarity. Hydrogen bonds are shown as yellow dashed lines. **E**, Superimposition of binding site of **9** (in dark blue and pink), **8** (in light blue and light pink), and **1** (in grey). Ligands and residues interacting with the ligand are shown as lines. Tyr82 is not shown for clarity.

Differences to compound 1 binding mode

Overall, the binding modes of **1** and **9** and **8** are very similar (**Figure 6e**). However, there are five main differences: (1) compound **1** does not form an intramolecular hydrogen bond similarly to our compounds. Instead, there is a possibility for an intramolecular hydrogen bond between the amide NH group and etoxy oxygen of **1**; (2) compound **1** does not form hydrogen bonds to Tyr82 or to Ser83 due to the absence of polar substituents on its 2-ethoxyphenyl moiety; (3) the hydrophobic interaction with Phe250 is likely weaker for **1** (distance 4.2 Å) than for **9** (4.0 Å) and **8** (4.0 Å) since Phe250 is positioned ca. 0.5-0.6 Å further away from the compound compared to the structures with **9** and **8**; (4) compounds **1** and **8** are not engaged in a hydrophobic interaction with Thr34; (5) compound **1** forms hydrophobic interactions with Phe232 via its cyclopropyl moiety, whereas the **9** and **8** methyl group of the sulfonamide is shorter and shielded from Phe232 by the sulfonamide oxygens. The last point is in line with the SAR of our compounds as well, where cyclopropyl is tolerated in this position and results in slightly better activities (e.g. **3** vs. **2**).

Structural basis for positive allosteric modulation by 9 and 8

As reported by Liu et al. [12], the positive allosteric modulation of BAM8-22 by **1** relies on two main structural determinants: (1) direct hydrophobic interaction of 1 with Tyr17 of BAM8-22, and (2) a strengthened charge interaction between Arg20 of BAM8-22 and Asp177 and Glu157 of MRGPRX1, resulting from **1**-binding-induced conformational changes of Tyr99 and Phe236[12]. Consistent with determinant (1), **9** and **8** likewise engage in direct hydrophobic interactions with Tyr17 of BAM8-22 at comparable distances. Regarding determinant (2), in the MRGPRX1–BAM8-22 cryo-EM structure (PDB: 8DWC;[12]), only two weak hydrogen bonds are observed between Arg20 and Glu157 (3.5 Å each), whereas in the corresponding **1**-bound structure (PDB: 8DWG;[12]), three hydrogen bonds with more favorable distances are formed between Arg20 and both Glu157 (3.2 Å, 3.3 Å) and Asp177 (3.2 Å) (**Supplementary Information Figure S5 A–B**). Notably, in the presence of **9** or **8**, Arg20 of BAM8-22 similarly forms three hydrogen bonds with Glu157 and Asp177, but with even shorter and thus more favorable distances (**9**: 2.6 Å, 2.9 Å, 3.1 Å; **8**: 2.5 Å, 3.1 Å, 3.1 Å), suggesting that this interaction is further strengthened relative to the **1**-bound state (**Supplementary Information Figure S5 C–D**). Overall, **9** and **8** share the structural basis of **1**-mediated positive allosteric modulation and additionally exhibit a further strengthened Arg20–Glu157/Asp177 hydrogen bond network, providing a structural rationale for their activity as positive allosteric modulators of MRGPRX1.

Discussion

In this study, we report the discovery and characterization of novel small-molecule positive allosteric modulators (PAMs) of MRGPRX1 through an integrated workflow combining docking-based virtual screening, medicinal chemistry, functional pharmacology, SPR biosensing, and

cryo-EM. Incorporating explicit water molecules into our docking strategy enabled likely more accurate identification of ligand poses within the allosteric binding site of MRGPRX1, ultimately guiding the selection of several PAM chemotypes. These compounds displayed varying degrees of intrinsic agonism, and for the **2** compound family their predicted allosteric binding site within the 7TM domain was confirmed structurally.

A key achievement of this work was obtaining high-quality cryo-EM reconstructions of the active MRGPRX1–G protein complex with unusually strong density in the extracellular region, an area that typically suffers from low local resolution in active-state GPCR structures[7,12,18-20] making PAM placement challenging. Local resolutions of 2.4–2.6 Å for **9** and 2.6–2.7 Å for **8** allowed unambiguous modeling of the ligands and some insights of their surrounding hydration networks. This level of detail was enabled by optimized data collection and a processing strategy that improved particle orientation distribution and per-particle scaling prior to localized refinement. The resulting maps provided structural support for our computational predictions and compound design, including the presence of ligand-mediated interactions and ordered water molecules in the PAM pocket.

We also developed an SPR approach capable of probing ligand binding to a GPCR in complex with a Gqα subunit. To our knowledge, this represents the first example of an SPR assay measuring interactions with an active-state GPCR–G protein complex. This enabled state-dependent binding analyses, offering clearer insight into the mechanisms underlying allosteric modulation and allowing direct comparison of ligand interactions in active versus inactive receptor conformations. Such biophysical measurements complement traditional cellular assays by providing kinetic parameters that more precisely describe how PAMs bind to the active receptor conformation leading to receptor activation.

GPCRs comprise the largest class of drug targets in the human genome and are modulated by a substantial fraction of marketed therapeutics [1]. Despite this, much of the GPCRome remains pharmacologically unexplored, in part because orthosteric ligands often bind conserved sites where off-target effects are common [21]. Allosteric modulators offer a more selective alternative by tuning receptor response without competing with endogenous agonists. For this reason, functional assays must quantify not only the agonist-driven signaling (E_{max}, EC_{50}) but also the magnitude of modulation conferred by PAMs, such as shifts in agonist potency or efficacy. The combined approaches used here (state-resolved SPR, pharmacological profiling, and high-resolution cryo-EM) allowed us to correlate PAM binding behavior with functional outcomes and to define structural features that drive allosteric enhancement.

Together, these results demonstrate how integrating computational methods with complementary structural and biophysical techniques can accelerate the discovery of GPCR allosteric modulators. This workflow provides a framework for exploring the broader landscape of MRGPRX1 pharmacology and may be broadly applicable to other GPCRs where allosteric sites and activation-dependent conformations play key roles in ligand recognition.

Methods

Computational studies

To optimize the water molecule positions, a short molecular dynamics (MD) simulation of 100 ns was conducted using a protein complex (PDB ID: 8DWG) where G-protein was modelled as miniGq (sequence as reported by Nehme et al.) [13] using Scrödinger Suite 2022-4. The resulting receptor complex was oriented based on the OPM database [22] and embedded in the POPC lipid

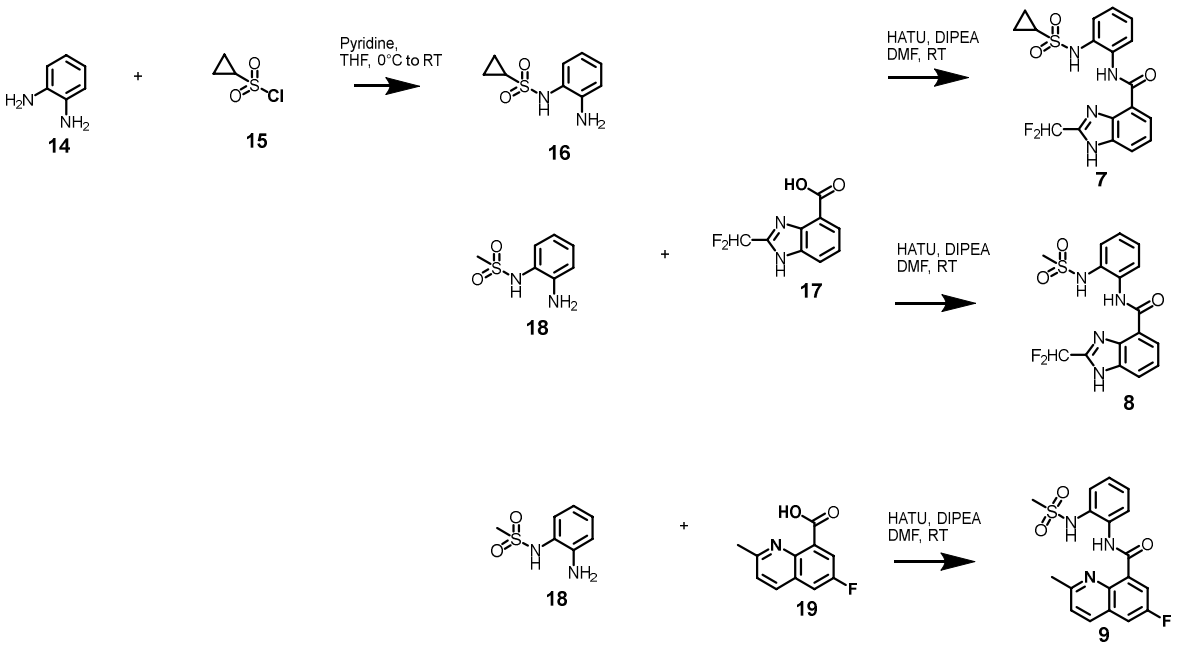
bilayer with TIP3p water molecules and 0.15 M NaCl using the system builder tool of Desmond (Schrödinger Suite 2022-4; **Supplementary Information Figure S6**). The standard membrane protein equilibration protocol of Desmond was utilized followed by 100 ns of production MD run with default parameters.

Every 10th frame was extracted from the MD trajectory excluding the first 50 ns to ensure the use of an equilibrated system. The frames, where **1** exhibited the desired interaction pattern with the receptor, and where there was at least one water molecule located within 2.5 Å of the sulfonamide nitrogen atom of **1** were selected. Docking grids were built utilizing Schrödinger suite 2023-1 centering the grid box on **1** and the separation power was tested using 13 active compounds [8,14] and 364 property matched decoys from the screening library (**Supplementary Information Figure S7**). The best performing grid was selected for the virtual screening.

The Enamine REAL database (April 2023 release), comprising approximately 2.539 billion compounds, was filtered to include molecules with a heavy atom count of 23–27, sLogP between 1 and 3.8, and no more than one stereocenter. This yielded a refined screening library of ca. 891 million compounds. HASTEN [15] together with Glide SP (Scrödinger Suite 2023-1) was utilized for virtual screening in four iterative rounds. Compounds with score cutoff of –10.0 and fulfilling the interaction criteria (hydrogen bonds with residues R79$^{2.57}$ and H254$^{7.35}$) were selected for post-processing. Post-processing included ligand strain energy cut-off 5 kcal/mol, ligand fingerprint similarity clustering, filtering out unwanted chemical scaffolds and visual inspection. Finally, 269 compounds were ordered from Enamin REAL.

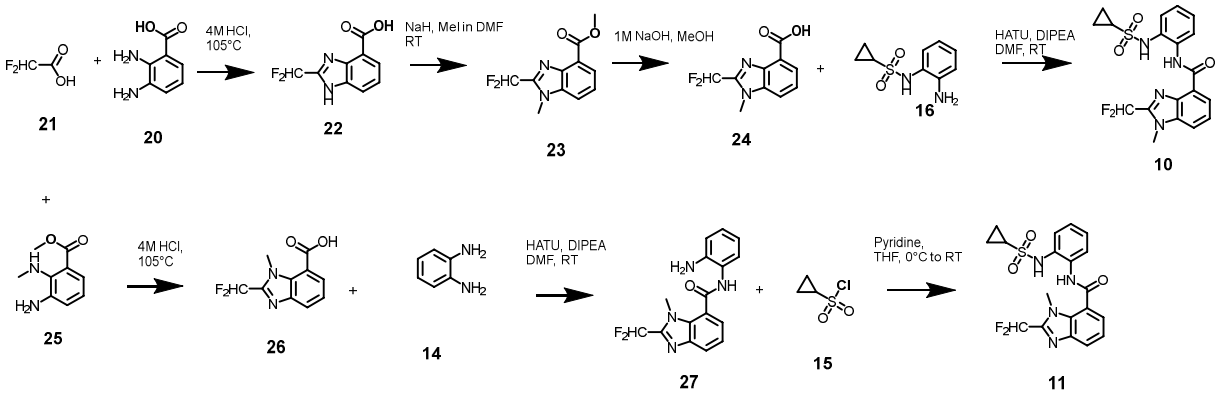
Chemistry

The target compound **7** was synthesized in two steps from o-phenylenediamine **14**: treatment with sulfonyl chloride **15** afforded N-(2-aminophenyl)cyclopropansulfonamide **16**, which was coupled with carboxylic acid **17** using HATU. Compounds **8** and **9** were similarly prepared via HATU-mediated coupling of **18** with the corresponding acids **17** and **19**, respectively. (Scheme 1)



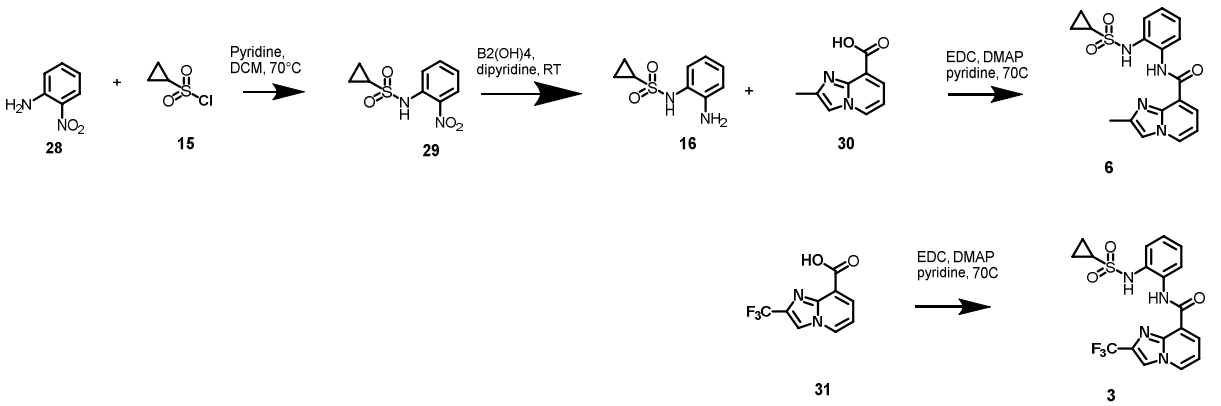
Scheme 1. Synthesis of Benzimidazole and Quinoline Derivatives (compounds **7**, **8** and **9**)

For the monomethylated target **10**, cyclization of **20** with acid **21** generated the benzimidazole core, which was selectively N-methylated and esterified to yield **23**; ester hydrolysis followed by HATU coupling with **16** furnished **10**. Likewise, cyclization of **25** with **21** provided **26**, which was coupled with **14** and treated with cyclopropanesulfonyl chloride **15** to afford the final compound **11** (Scheme 2).



Scheme 2. Synthesis of N-Methylated Benzimidazole Derivatives (compounds **10** and **11**)

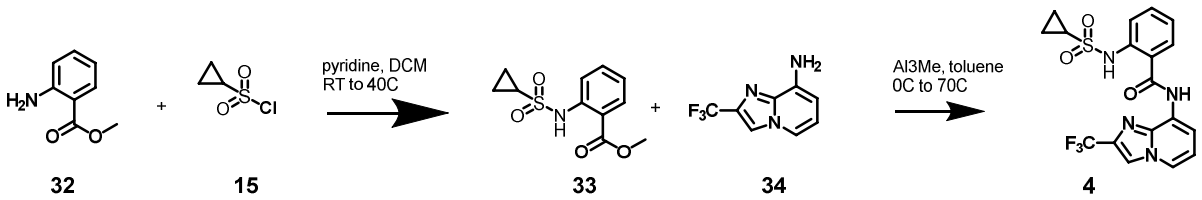
Target compounds **6** and **3** were prepared from nitroamine **28**. Treatment with sulfonyl chloride **15** lead to N-(2-nitrophenyl)cyclopropanesulfonamide **29**, which was reduced with hypoboric acid to afford N-(2-aminophenyl)cyclopropanesulfonamide **16**. Coupling with carboxylic acid **30** using EDC/DMAP led to compound **6**. A similar method was used to prepare target compound **3** from carboxylic acid **31**.



Scheme 3. Synthesis of Imidazopyridine Derivatives (compounds **3** and **6**)

Inverted amide target compound **4** was synthesized in two steps from 2-amino-phenylmethylcarboxylate **32**. Sulfonylation with sulfonyl chloride **15** afforded N-(2-

methylcarboxylate)cyclopropanesulfonamide **33**. Coupling with amine **34** under trimethylaluminum lead to target compound **4**.



32 **15** **33** **34** **4**

Scheme 4. Synthesis of Inverted Amide Imidazopyridine Derivative (compound **4**)

Compounds **2** and **5** have been purchased from Enamine REAL Space (Enamine Ltd.).

Cloning of constructs

Synthetic genes encoding full length MRGPRX1 (Q96LB2) were integrated into the baculovirus pVL1393 transfer vector [7]. All construct carried at the N-terminus an influenza hemaglutinin secretion tag followed by a flag-tag BRIL fusion and a PreS cleavage site. The construct for the SPR experiment carried a C-terminal AVI tag.

Synthetic genes encoding different G proteins Gqα (P50148), Gß (P62873) and Gγ (P59768) were integrated into the baculovirus pVL1393 transfer vector. The first amino acids were substituted by amino acid 1-18 from GNAI, followed by an engineered Gqα sequence [7]. The GNB1 construct carried an N-terminal His-tag followed by PreS cleavage site.

Adeno-associated viral vectors for the expression of full length human MGRPRX1 (VectorBuilder, #VB220628-1140aea) or EGFP control (VectorBuilder, #VB220629-1654pve) were cloned and packaged in AAV serotype 1 particles by VectorBuilder Inc.

To create the cell line stably expressing human MRGPRX1, HEK293 cells were transfected with the plasmid vector encoding full length MRGPRX1 and puromycin selection cassette (VectorBuilder, #VB220629-1340ppq). After puromycin (1 µg/ml) selection for 4 weeks, a clonal cell population was obtained by serial dilutions method. Successful expression of MRGPRX1 clone was confirmed by mass spectrometry and functional studies.

Expression of MRGPRX1 and MRGPRX1 complexes in insect cells

All constructs were expressed in SF9 insect cells (Expression Systems) using flashback baculovirus system (Oxford expression Technologies) according to manufacturer's instructions. SF9 cells were cultivated in suspension in ESF21 (Expression System). In small scale test expression experiments best expression condition to obtain soluble folded MRGPRX1 alone or in complex with G proteins were identified, by infected of SF9 cells at a density of 2.0 x 106 cells/mL with high-titer viral stock at different multiplicities of infection (m.o.i). Cells were harvested by centrifugation 48 or 72 hours after infection and stored at -20°C until purification.

For large scale recombinant protein production of MRGPRX1 and MRGPRX1 in complex with G proteins. Sf9 cells at densities of 2.0 x 106 cells/mL were infected with high-titer viral stock at a multiplicity of infection (m.o.i) of 0.3. For complex formation cells were infected with up to 4 different viruses (MRGPRX1/ Gqα /Gß Gγ). Cells were incubated for 48 h at 27 °C in a cell wave bag at 22 rpm, harvested by centrifugation, flash frozen and stored at -70°C until use.

Protein purification

The overall purification steps were carried out at 4°C or on ice. Biomass corresponding to 2 liters of insect cell culture was thawed on ice and resuspended in lysis buffer (50mM HEPES pH 7.5;

100mM NaCl, 2mM MgCl2, 5mM CaCl2,10µM BAM8-22, 5% glycerol) supplemented with cOmplete protease inhibitor Cocktail (Roche Applied Science).

Purification of MRGPRX1/ Gqα/Gβ/Gγ/scFV16 complex for cryo-EM grid preparation

The receptor was solubilized by addition of 0.8% (w/v) LMNG (Anatrace), 0.2% (w/v) GDN (Anatrace) 0.1% (w/V) CHS (Sigma), 10 strokes in a glass douncer tissue followed by 1 hour incubation under gentle agitation and at 4°C. For MRGPRX1 G-protein complexes purification Apyrase 25U/ml was added to the solubilization buffer. The insoluble fraction was removed by centrifugation (150 000g, 45 min). Detergent solubilized MRGPRX1 constructs were captured by gravity flow on a 2 ml M2 resin (Anti-Flag M2-agraose, Sigma) pre-equilibrated with binding buffer (20mM HEPES pH 7.5, 100mM NaCl, 2mM MgCl2, 5mM CaCl2, 50µM BAM8-22, 0.08%LMNG/0.02%GDN/0.01%CHS). M2 resin was washed with 10 CV wash buffer (20mM HEPES pH 7.5, 300mM NaCl, 2mM $MgCl_2$, 5mM CaCl2, 50µM BAM8-22, 0.0016%LMNG/0.004%GDN/0.002%CHS) followed by a second washing step with 10CV wash buffer supplemented with 5mM and eluted with elution buffer (20mM HEPES pH 7.5, 100mM NaCl, 2mM $MgCl_2$, 50µM BAM8-22, 0.0016%LMNG/0.004%GDN/0.002%CHS, 0.4mg/ml flag peptide). Protein concentration was determined using A280. 1.5 molar equivalents of scFV16 were added to the complex. The mixture was incubated on ice for 1 hour and then the sample was subsequently concentrated with a 100-kDa Vivaspin Turbo concentrator (Sartorius) to a final volume of 500 µl. Samples was further purified by size-exclusion chromatography using a Superose 6 Increase 10/300 GL column (GE Healthcare) pre-equilibrated with gel filtration running buffer (20mM HEPES pH 7.5, 100mM NaCl, 2mM $MgCl_2$, 10µM BAM8-22, 0.00016%LMNG/0.0004%GDN/0.0002%CHS). Fractions containing both the GPCR and the

antibody fragment were pooled. Compounds BAM8-22 and **8** or **9** were added to 100 µM, respectively. The pooled sample was then concentrated down to the minimum volume (~40 µl) for cryo-EM grid preparation.

Purification of MRGPRX1 and MRGPRX1/ Gqα complex for SPR experiments

Purification procedure was the same as above, but the detergent composition was different. For solubilization 0.5% (w/v) LMNG (Anatrace), 0.05% (w/V) CHS (Sigma) were added, for all other steps 0.01% LMNG and 0.001 % CHS were used. The final SEC buffer was 50mM HEPES pH 7.4, 100mM NaCl, 5mM $MgCl_2$, 0.01%/0.001% LMNG/CHS, 5% Glycerol. The MRGPRX1 containing peak fractions were pooled, flash frozen and stored at -70°C.

Surface Plasmon Resonance (SPR) Assay

Biotinylated MRGPRX1, MRGPRX1/ Gqα and A_2AR were captured at 16°C on a SA-Chips. Immobilization buffer contained 50mM HEPES pH 7.4, 100mM NaCl, 5mM $MgCl_2$, 0.01%/0.001% LMNG/CHS, 5% Glycerol. Obtained immobilization levels were between 3000 and 5000 RU. A Biacore T200 (Cytivia) instrument was used for all experiments. Binding assays were performed at 16°C, running buffer contained 50mM HEPES pH 7.4, 100mM NaCl, 5mM MgCl2, 0.01%/0.001% LMNG/CHS, 5% Glycerol and 2% DMSO, in some experiments the running buffer was supplied with 5µM BAM8-22 peptide. Compounds were injected at a concentration series 19-2500nM, flow rate of 10µl/min, with association time of 90 sec and dissociation time of 180 sec or association time of 60 sec and dissociation time of 120 sec. For evaluation and fitting of data insight software (Cytivia) was used. Sensograms are shown in **Figure**

2 and **Figure 3**. Details for SPR data analysis are summarized in **Supplementary Information Table S2**.

Functional assays

TR-FRET assays AGO / PAM

Agonistic or Positive Allosteric Modulator (PAM) activities of compounds were quantified using a time-resolved fluorescence resonance energy transfer (TR-FRET) assay with the IP-One Gq Detection Kit (Revvity, Hamburg, Germany; #62IPAPEC). This assay measures the accumulation of endogenous IP1, which is produced upon activation of Gq-coupled GPCRs, using a competitive TR-FRET approach. Endogenous IP1 competes with the fluorescence-acceptor labeled IP1-d2 for binding to a terbium-labeled anti-IP1 antibody. The TR-FRET signal decreases with increasing concentrations of endogenous IP1. To assess agonistic stimulation, frozen HEK-X1 cells were rapidly thawed and transferred to warm assay medium (DMEM, high glucose, Gibco #61965; 10% FBS Superior, Sigma #S0615; 100 U/ml Penicillin, 100 µg/ml Streptomycin, Gibco #15140; 1 µg/ml Puromycin, Gibco #A11138-03). Following centrifugation at 200 x g for 5 minutes, the cell pellet was resuspended in assay medium to obtain a concentration of 4 x 10^6 cells/ml. 2 µl/well of this cell suspension were dispensed (using a Multidrop™ Combi, Thermo Fisher Scientific, Waltham, USA) into a 384-well assay plate (Greiner; #784075) pre-loaded with 50 nl/well of compound solution in 100% DMSO (11-point 1:3.5 serial dilution from 2 mM to 7.25 nM). The reaction was started by adding 2 µl/well of either: 1) 1x stimulation buffer + 0.01% Pluronic for compound wells and DMSO wells as neutral controls or 2) BAM8-22 diluted to 50 µM in the same buffer (resulting in final concentration of 25 µM; MedChem Express; #HY-P1241) for stimulator control wells. After 60 minutes of incubation at 37°C, 5% CO2 in a humidified incubator, the

reaction was stopped by adding 2 µl/well lysis & detection buffer containing the detection reagents (IP1-d2 and anti-IP1-Tb diluted 1:40 in lysis & detection buffer). An additional 60-minute incubation at room temperature was performed to allow for complete lysis. TR-FRET signal (ex 337 nm; em 665 nm/ 620 nm) was measured using a PHERAstar microplate reader (BMG Labtech, Ortenberg, Germany). The TR-FRET ratio values (665 nm/620 nm) were normalized between neutral controls (DMSO; 0% activation) and stimulator controls (25 µM BAM8-22; 100% activation). EC_{50} values of dose response curves were calculated by fitting the normalized data to a four-parameter logistic equation using the Genedata Screener software (Genedata AG, Basel, Switzerland).

To identify PAMs, the same assay procedure was used with the following modifications: The 1x stimulation buffer + 0.01% Pluronic solution was solely used as blank control and added to DMSO control wells. The agonist working solution (1x stimulation buffer + 0.01% Pluronic + 2x EC10-20 of BAM8-22) was rather added to all compound and neutral control wells. The respective EC_{xx} of the agonist BAM8-22 was calculated based on median values of blank, neutral and stimulator controls.

Combined FLIPR AGO / PAM assay

The agonistic and PAM potential of compounds were also assessed kinetically by FLIPR®Tetra or FLIPR®Penta (Fluorometric Imaging Plate Reader, Molecular Devices LLC, San Jose, USA) measuring release of calcium ions into the cytosol in real time. Cells were loaded with a cell-permeable calcium-sensitive dye (FLIPR Calcium 6 Assay Kit, Molecular Devices LLC, #R8190 or #R8191), which increases fluorescence upon calcium binding. A non-cell-permeable quencher is applied with the dye to suppress extracellular fluorescence (coming from e.g. dye molecules

outside of the cells). Following compound addition, the fluorescence intensity is monitored to detect agonistic potential. Subsequently, an agonist at low concentrations (EC_5-EC_{25}) is transferred to determine whether compounds which did not show agonism before can act as PAMs.

In the combined FLIPR Ago/PAM assay, HEK-X1 were detached, washed and resuspended in an appropriate volume to obtain a cell working solution of 4 x 10^5 cells/ml in assay medium (DMEM, high glucose, Gibco #61965; 10% FBS Superior, Sigma #S0615; 100 U/ml Penicillin, 100 µg/ml Streptomycin, Gibco #15140; 1 µg/ml Puromycin, Gibco #A11138-03). 25 µl/well of this cell suspension were dispensed into a poly-D-lysine (PDL)-coated 384-well plate (Corning, #354663), followed by overnight incubation at 37°C, 5% CO_2 in a humidified incubator.

On the day of the assay, medium was discarded with a Blue®Washer, 20 µl/well loading dye (component A from kit dissolved with equal parts component B and hERG-ringer buffer + 0.02% Pluronic) were gently added to the assay plate. After 30 minutes incubation at 37°C, 5% CO2 and up to 30 minutes at room temperature, agonist measurement was started on FLIPR®Tetra or FLIPR®Penta with a 10 sec baseline (Ex/Em: 470-495/515-575 nm).

During the incubation time, a 384-well compound plate (Greiner, #784076), pre-loaded with 150 nl/well of serially diluted compounds in 100% DMSO (10-point 1:3 dilution from 5 µM to 254 nM), was filled with 13 µl/well of the following solutions: 1) Solely hERG-ringer buffer (10 mM Hepes pH 7.5, 143 mM NaCl, 1.2 mM MgCl2, 1.8 mM CaCl2, 4 mM KCl, 5 mM Glucose, adjusted to pH 7.4) + 0.01% Pluronic for all compound and neutral control wells. 2) hERG-ringer buffer + 0.01% Pluronic with 3x EC100 BAM8-22 for stimulator control wells of agonist assay and 3) hERG-ringer buffer + 0.01% Pluronic with 4x EC100 of a PAM, not exhibiting agonism at this concentration, for stimulator control wells of PAM assay.

10 µl/well from this prepared compound plate were transferred to the assay plate during continuous fluorescence acquisition for up to 120 seconds with 1 second intervals followed by further 60 seconds with 5 seconds intervals. Afterwards, the assay plate was incubated another 30 minutes at room temperature. The PAM assay was started again with a 10 seconds baseline measurement (Ex/Em: 470-495/515-575 nm). Then 10 µl/well 4x$EC_{10\text{-}30}$ BAM8-22 agonist solution was added and the plate continued to be measured up to 120 seconds with 1 second intervals followed by further 60 seconds with 5 seconds intervals. For both assays, Max-Min from the whole kinetic trace was calculated and normalized between neutral controls (set to 0% activation, Agonist assay: buffer no agonist, PAM assay: buffer with EC_{10}-EC_{30} BAM8-22) and stimulator controls (set to 100% activation, Agonist assay: EC_{100} BAM8-22, PAM assay: PAM in saturating concentration without sign of agonism). To analyze dose response curves, EC_{50} values were calculated by fitting the normalized data to a four-parameter logistic equation using the Genedata Screener software (Genedata AG, Basel, Switzerland).

FLIPR BAM8-22 shift assay

The FLIPR BAM8-22 shift assay was performed according to the procedure of the FLIPR PAM assay, with the following changes: The same test compound was diluted in dose response series in several rows on the assay plate. Instead of adding a single BAM8-22 solution to all wells during the PAM assay measurement in the FLIPR®, a dose-response series of BAM8-22 was applied: Each well received 10 µl of a 4x concentrated BAM8-22 solution (11-point 1:3 dilution series, ranging from 400 nM to 6.8 pM, plus buffer-only control) in hERG-ringer buffer + 0.01% Pluronic. The concentration-response data were analyzed without normalization in the GraphPad Prism software (GraphPad Software, Boston, USA).

Rat dorsal root ganglia (DRG) cultures

All animal studies were carried out in accordance with the EU Directive 2010/63/EU for animal experiments and were approved by the Regional State Administrative Agency of Southern Finland (approval number ESAVI/33509/2023). Adult Han/Wistar rats provided by Charles River, Germany, between the age of 4-10 weeks were sacrificed by CO_2 and their lumbar (L1-L6) DRGs collected in ice-cold Hibernate A medium (Gibco, #A1247501). The DRGs were chemically dissociated first by incubating them for 45 minutes in collagenase (ThermoFisher, #17101015) and then 15 minutes in 0.05% trypsin (Gibco, #15400-054). After this, trypsin was inhibited using Neurobasal medium (Gibco, #21103049) supplemented with 10% fetal bovine serum (Sigmal-Aldrich, #F7524), 2% B27 (Gibco, #17504044), 1% L-glutamine (Sigma-Aldrich, G7513) and 1% penicillin-streptomycin (Gibco, #15140122). Mechanical dissociation was done using 1 ml syringes and 18G or 22G needles. After mechanical dissociation, the cell suspension was filtered through a 70 μM nylon cell strainer (Sigma-Aldrich, #CLS431751) and the media was changed to Neurobasal supplemented with 2% B27, 1% L-glutamine, 1% penicillin-streptomycin and 200 ng/ml NGF (R&D systems, #256-GF-100). 25% of the media was replenished every 4-5 days.

For the expression of EGFP and human MRGPRX1, rat DRG cultures on 96 well plates were transduced at 12-14hr after isolation with AAV vectors diluted in DRG culture media at final titer of 5×10^7 genome copies/ul. After 7-10 days the cells were checked for EGFP fluorescence and taken for electrophysiological experiments.

Electrophysiology

Whole-cell patch clamp recordings of DRG neuron calcium currents were performed at room temperature using solutions and a modified voltage protocol from Li et al [5]. Cultured rat DRG

neurons were harvested and drops of the cell suspension were pipetted into the recording chamber of a Dynaflow Resolve chip (Fluicell, Sweden). Fluorescent neurons were patched with pipettes pulled from borosilicate glass and filled with a solution consisting of (in mM): 140 tetraethylammonium chloride, 1 $MgCl_2$, 10 HEPES, 10 EGTA, 0.5 Na_2GTP, and 3 MgATP (pH 7.2; osmolarity 290 ± 2 mOsm). The neuron was then moved to the outflow of a channel-perfusing extracellular solution consisting of (in mM): 130 NMDG-Cl, 5 $BaCl_2$, 1 $MgCl_2$, 10 glucose, and 10 HEPES (pH 7.4 with NMDG; osmolarity 300 ± 3 mOsm). Patch Series resistance (by 40%) and capacitance were compensated with an Axopatch 200B amplifier (Molecular Devices). From a holding potential of -80 mV cells were depolarised to -40 mV for 30 ms to activate LVA Ca^{2+} channels, followed by a step to -60 mV for 50 ms and a depolarisation to -10 mV for 30 ms to activate HVA Ca^{2+} channels. This protocol was repeated every 10 s. Recordings were filtered at 2 kHz and sampled at 10 kHz. Data analyzed with pClamp 11.4 software (Molecular Devices).

Cryo-EM

Grid preparation and image collection

For the preparation of cryo-EM grids, 3.5 μL of sample at a concentration of 11 mg/mL for MRGPRX1-**9** or 8.2 mg/mL for MRGPRX1-**8** was applied onto glow-discharged holey carbon grids (QuantiFoil R1.2/1.3 200 Cu mesh) in a Vitrobot chamber (Thermo Fisher Vitrobot Mark IV). The Vitrobot chamber was set to 100% humidity at 4 °C. After sample application, the grid was blotted for 5 s with blot force 0 for MRGPRX1-**9** or blot force10 for MRGPRX1-**8** and plunged into liquid ethane. Grids were stored in liquid nitrogen for condition screening and data collection usage.

Grid screening was performed on a 200 kV Glacios (Thermo Fisher) operated at 200 kV with a Selectris X energy filter (operated at a slit width of 10 eV). The best grid of MRGPRX1- **8** was subjected to an automated data collection using the same microscope. The microscope was operated with a nominal magnification of 130.000x in counting mode, corresponding to a pixel size of 0.87 Å. A total of 6.297 movies were collected by a Falcon 4i direct electron detector at a defocus ranging from – 0.6 µm to – 2.0 µm using the software SerialEM v4.2.0beta[23]. Each movie comprised of 1.404 fractions with at total does of 50 $e^-/Å^2$ and a total exposure time of 4.6 s. The best grid of MRGPRX1-**9** was subjected to an automated data collection using a 300 kV Titan Krios G4 (Thermo Fisher) with C-FEG and Selectris X energy filter (operated at a slit width of 10 eV). The microscope was operated with a nominal magnification of 165.000x in counting mode, corresponding to a pixel size of 0.731 Å. A total of 12.805 movies were collected by a Falcon 4i direct electron detector at a defocus ranging from – 0.7 µm to – 2.0 µm using SerialEM v4.2.0beta. Each movie comprised of 666 fractions with at total does of 50 e/Å2 and a total exposure time of 2.1 s.

Data processing

*MRGPRX1-**9** dataset*

All initial processing steps were performed with Relion 5.0[24]. All 12.805 movies were aligned using Relion 5.0 own implementation of MotionCor2. Contrast Transfer Function (CTF) parameters were estimated by CTFFIND-4.1[25]. Manual image curation resulted in 12.678 images. Particle picking with TOPAZ [26] pretrained model resulted in 6.022.110 particles. Three rounds of 2D classification resulted in 106.729 high-quality particles that were used to train TOPAZ. TOPAZ picking after training resulted in 6.768.637 particles. Particles were extracted at a box size of 336

px and four-times binned and subjected to three rounds of reference-free 2D classification, resulting in 349.408 particles. Ab-initio model generation, followed by two rounds of 3D classification, full unbinning, CTF refinement. Bayesian polishing, and auto-refinement resulted in 123.374 particles and a 3D map of 2.92 Å average resolution. This map was used as a 3D reference for a large 3D classification of 1.839.633 particles (selected after the first round of 2D classification), resulting in 331.008 particles. Subsequent particle reextraction to full unbinning at a box size of 360 px, CTF refinement, Bayesian polishing, auto-refinement, and post processing lead to a 3D map of 2.74 Å resolution. The particles stack and 3D map were transferred to cryoSPARC v4.5.3[27] where all subsequent jobs were performed. Non-uniform 3D refinement (NUR). CTF refinement, and again NUR resulted in a 3D map of 2.50 Å resolution. To further improve the quality of the particle stack, rebalancing orientations and subset particles by per-particle scale were performed, which improved the conical FSC area ratio (cFAR) value from 0.54 to 0.61 and led to 129.960 particles and a 3D map of 2.33 Å average resolution, with a local resolution of the ligand density of 2.75-2.90 Å. Local refinement with a mask around the transmembrane region of the GPCR resulted in a 3D map with an average resolution of 2.63 Å and a local resolution at the ligand density of 2.40-2.60 Å. Map sharpening was performed with DeepEMhancer[28].

*MRGPRX1-**8** dataset*

All initial processing steps were performed with Relion 5.0. All 6.297 movies were aligned using Relion 5.0 own implementation of MotionCor2. Contrast Transfer Function (CTF) parameters were estimated by CTFFIND-4.1. Manual image curation resulted in 4.106 images. Particle picking with TOPAZ pretrained model resulted in 3.670.412 particles. One round of 2D

764 classification resulted in 585.650 high-quality particles that were used to train TOPAZ. TOPAZ
765 picking after training resulted in 2.691.949 particles. Particles were extracted at a box size of 280
766 px and four-times binned, and subjected to two rounds of reference-free 2D classification, resulting
767 in 447.219 particles. Ab-initio model generation, followed by two rounds of 3D classification, full
768 unbinning, CTF refinement, Bayesian polishing, and auto-refinement resulted in 281.083 particles
769 and a 3D map of 2.98 Å average resolution. This map was used as a 3D reference for a large 3D
770 classification of 2.691.949 particles (all particles after TOPAZ picking), resulting in 567.087
771 particles. Subsequent particle reextraction to full unbinning at a box size of 288 px, Bayesian
772 polishing, auto-refinement, and post processing lead to a 3D map of 2.91 Å resolution. The
773 particles stack and 3D map were transferred to cryoSPARC v4.5.3 where all subsequent jobs were
774 performed. Non-uniform 3D refinement (NUR), two rounds of heterogeneous refinement, and
775 NUR reduced the number of particles to 390.769 and produced a 3D map of 2.71 Å resolution.
776 Rebalancing orientations and subset particles by per-particle scale improved the cFAR value from
777 0.48 to 0.53 and led to 234.760 particles and a 3D map of 2.72 Å. CTF refinement followed by
778 NUR resulted in a final average resolution of 2.63 Å, with a local resolution of the ligand density
779 of 2.70-2.90 Å. Local refinement with a mask around the transmembrane region of the GPCR
780 resulted in a 3D map with an average resolution of 2.87 Å and a local resolution at the ligand
781 density of 2.60-2.70 Å. Map sharpening was performed with DeepEMhancer.
782
783 **Model building and refinement**
784 The coordinates of PDB-ID 8DWG [12] were used as the initial model for model building. The model
785 was docked into the EM density in COOT 0.9.6 [29] sing the Jiggle-fit function. The fitted model
786 was iteratively optimized by manual adjustment in COOT followed by refinement against the EM

787 map using REFMAC5[30] (Refmac 5.8.0430 wrapped in Servalcat v 0.2.137[31]). Model validation
788 was performed using Molprobity[32]). Refinement statistics are summarized in **Supplementary**
789 **Information Table S1**.

Acknowledgments: The authors would like to thank Jubilant Biosys, Greater Noida, India, for the syntheses of compounds **3**, **4** and **6**, and the reference compounds **1**, **12** and **13**.

Author contributions:

Conceived the project: ATM, MJ, LL

Synthesized compounds: YW, DN

Performed experiments: ATM, AU, CJ, MI, HC, AD, KNR, VP, LL

Analyzed data: ATM, AU, MJ, KNR, VP, DN, HM, LL

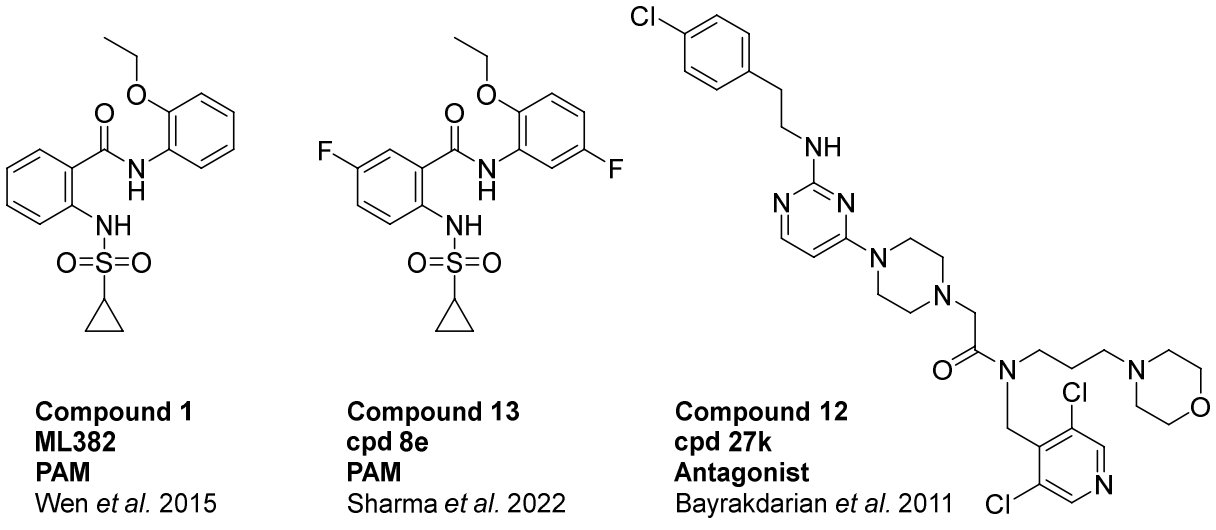
Wrote the manuscript and prepared the figures: ATM, AU, KNR, VP, DN, LL

Contributed to writing: MJ, YW, CJ, HM, HC, AD

Competing interests: The authors declare that they have no known financial or personal relationship that could have influenced the work reported in this paper. ATM, MJ, CJ, MI, HC, AD and LL are employed at Orion Corp. AU, YW, KNR, VP, ND and HM are employed at Nuvisan ICB GmbH.

Data and materials availability: The datasets generated during and/or analyzed during the current study are available on reasonable request. Molecular dynamics simulation snapshots evaluated as part of docking grid generation are provided as supplementary files. The cryo-EM structures have been deposited to Protein Data Bank (PDB) and Electron Microscopy Data Bank (EMDB) with following accession codes: MRGPRX1-complex with compound **9** (global refined structure), PDB ID: 30PS, EMDB: EMD-57927; MRGPRX1-complex with compound **9** (local refined structure), PDB ID: 30PX, EMDB: EMD-57929; MRGPRX1-complex with compound **8** (global refined structure), PDB ID: 30PZ, EMDB: EMD-57936; MRGPRX1-complex with compound **8** (local refined structure), PDB ID: 30QB, EMDB: EMD-57939.

Supplementary Figures and Tables

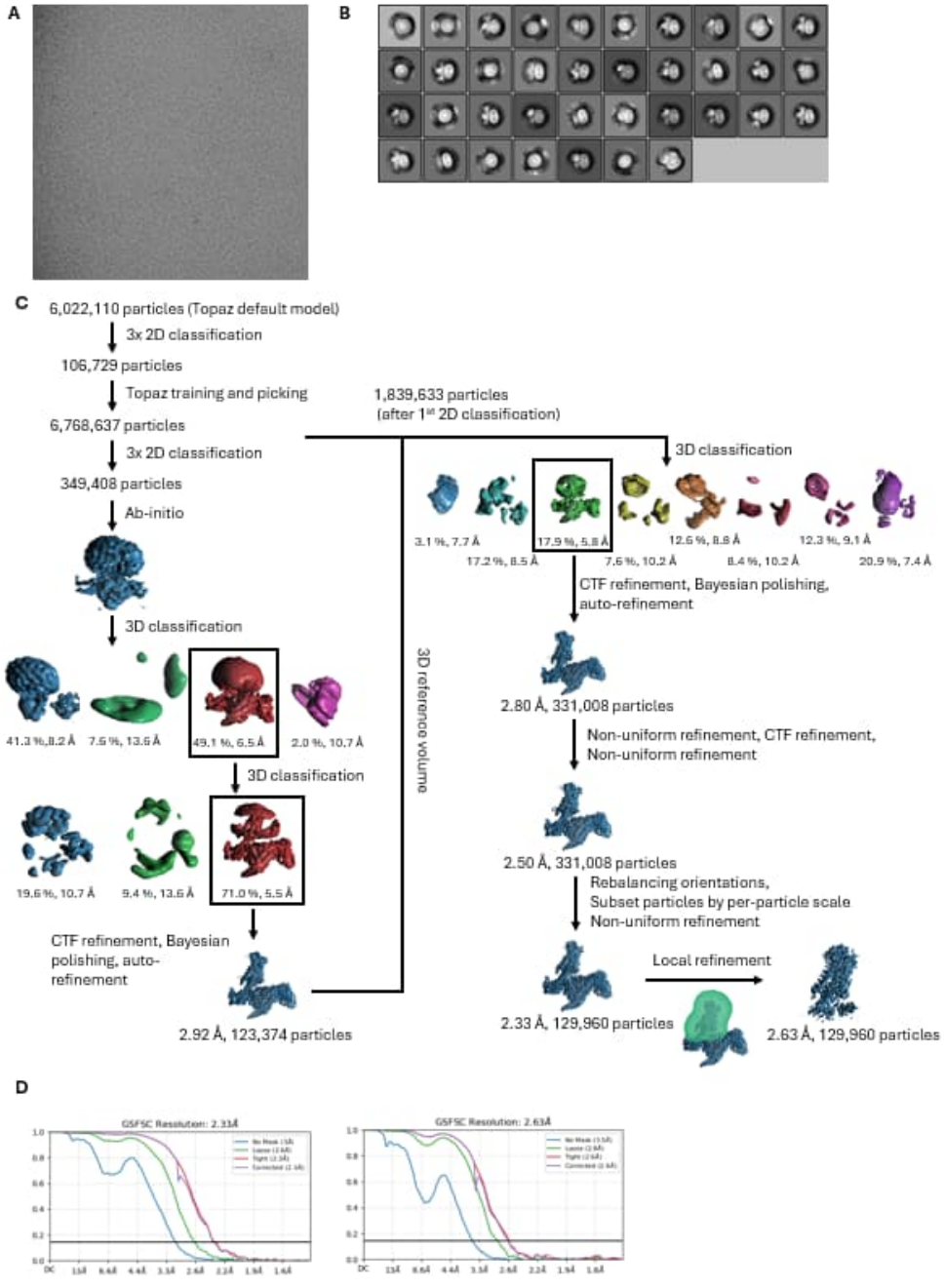


Compound 1
ML382
PAM
Wen *et al.* 2015

Compound 13
cpd 8e
PAM
Sharma *et al.* 2022

Compound 12
cpd 27k
Antagonist
Bayrakdarian *et al.* 2011

Figure S1: Reference compounds utilized in this study



817

818 **Figure S2: Cryo-EM processing of MRGPRX1-9**

819 **(A)** Representative micrograph. **(B)** representative 2D classes. **(C)** cryo-EM processing scheme.

820 and **(D)** FSC curves for MRGPRX1-**9** cryo-EM structure.

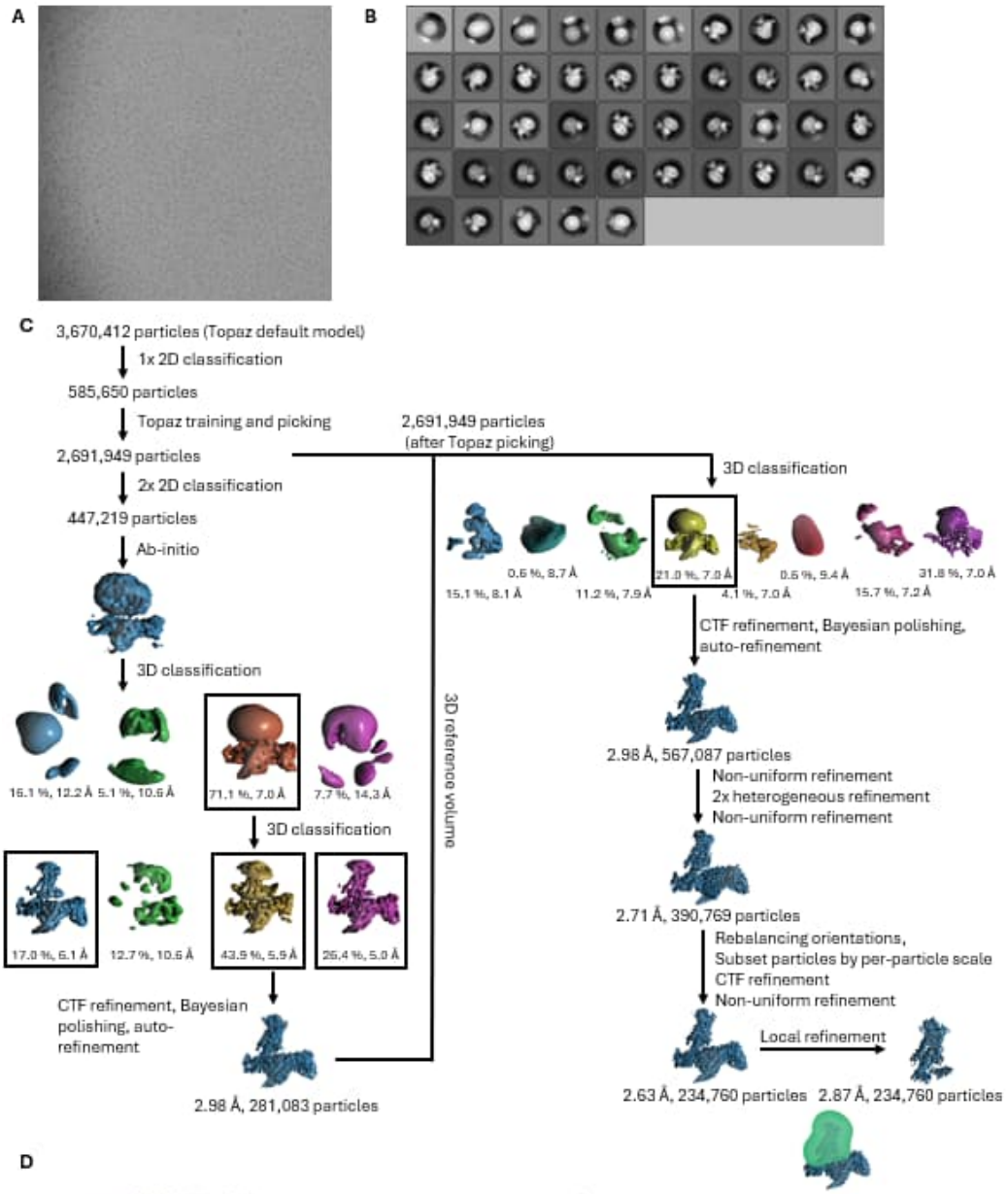


Figure S3: Cryo-EM processing of MRGPRX1-8

(A) Representative micrograph. **(B)** representative 2D classes. **(C)** cryo-EM processing scheme. and **(D)** FSC curves for MRGPRX1-**8** cryo-EM structure.

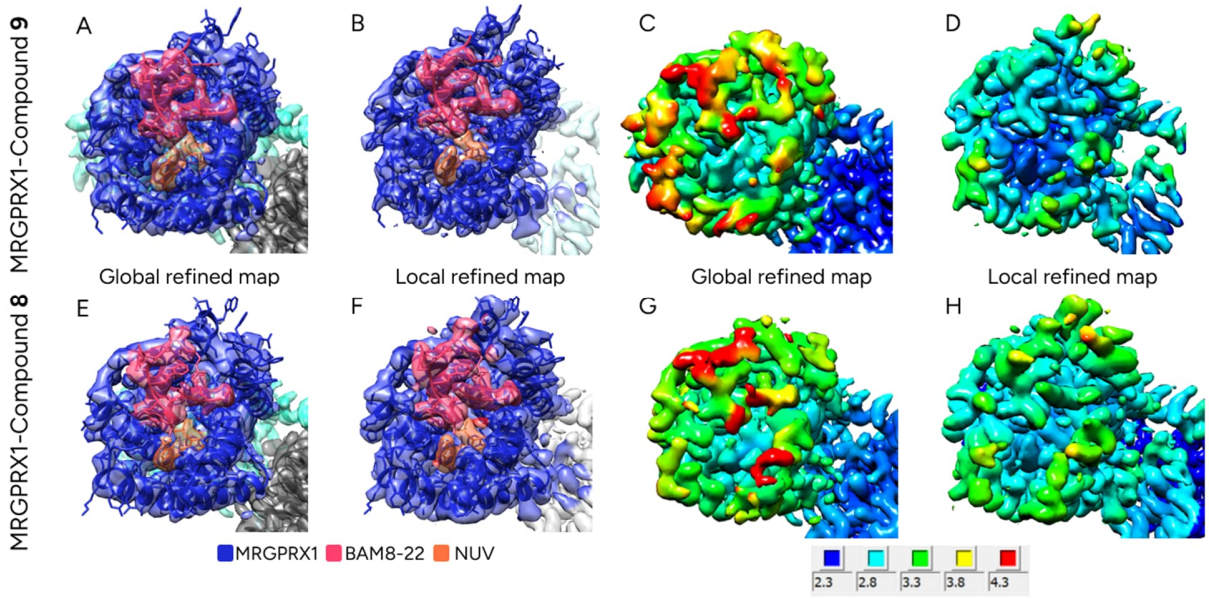


Figure S4: Comparison of cryo-EM densities of BAM8-22 and PAM binding region between global and local refined cryo-EM maps

(A-D) Comparison of global refined **(A)** and local refined **(B)** sharpened cryo-EM density maps and corresponding local resolution maps **(C and D)** around BAM8-22 and **9** binding region. **(E-H)** Comparison of global refined **(E)** and local refined **(F)** sharpened cryo-EM density maps and corresponding local resolution maps **(G and H)** around BAM8-22 and **8** binding region. All maps are contoured to rmsd 1.0. MRGPRX1 is colored in dark blue, BAM8-22 in pink, and **9** and **8** in orange (in A, B, E, F).

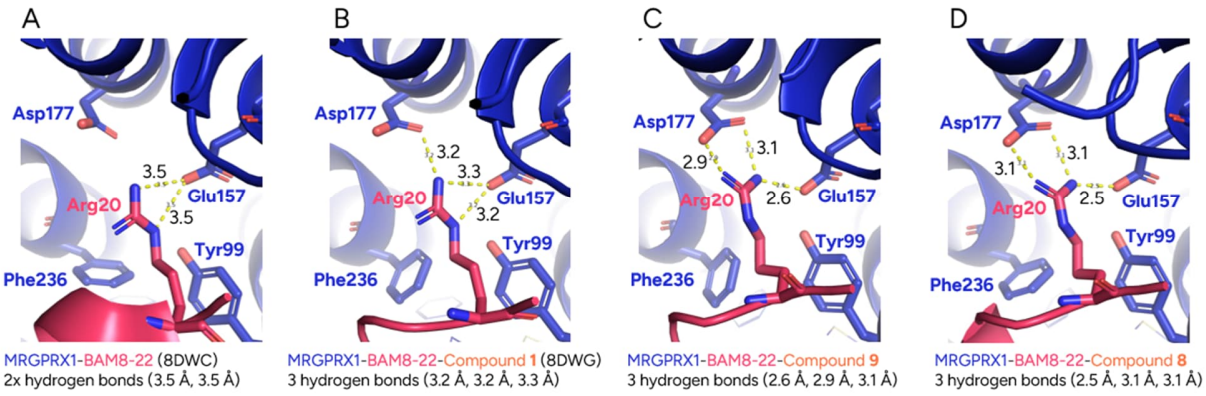
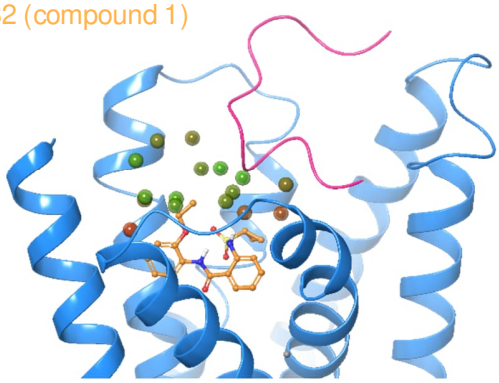


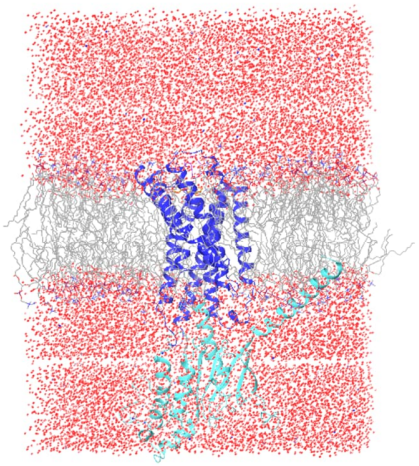
Figure S5: Structural basis for positive allosteric modulation by NUV763 and NUV736

Hydrogen bond network between BAM8-22 Arg20 and MRGPRX1 Glu157 and Asp177 in **(A)** MRGPRX1-BAM8-22 (8DWC), in **(B)** MRGPRX1-BAM8-22-**1** (8DWG), in **(C)** MRGPRX1-BAM8-22-**9**, and in **(D)** MRGPRX1-BAM8-22-**8**. Residues involved in the interaction (Arg20, Glu157, Asp177) or involved in transmitting the conformational change caused by PAM binding (Tyr99, Phe236) are shown as sticks. Hydrogen bonds are shown as dotted lines. MRGPRX1 is colored in dark blue and BAM8-22 in pink.

852

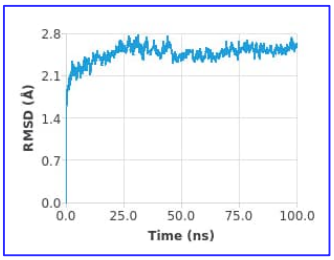
MRGPRX1 protein
MiniGprotein
BAM8-22 peptide
ML382 (compound 1)

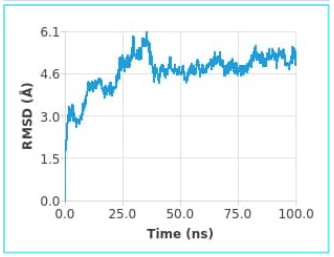


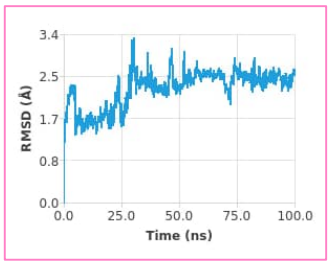


Simulation box (orthorhombic)	Total number of atoms	Number of water molecules	Salt concentration	Number of lipid molecules
99 Å * 74 Å * 126 Å	90624	20060 (TIP3p)	0.15 M NaCl	164 (POPC)

Description	Temperature	Time and timestep	Restraints
Brownian dynamics NVT	10 K	50 ps, 1 fs	Solute (heavy atoms): 50 kcal/mol*Å^2
Brownian NPT, H_2O barrier	100 K	20 ps, 2 fs	Membrane (non-H) restrained in z, protein heavy atoms: 20 kcal/mol*Å^2
NPgT (MTK, Nose-Hoover), H_2O barrier	100 K	100 ps, 2 fs	Membrane headgroups restrained in z, protein heavy atoms: 10 kcal/mol*Å^2
NPgT (MTK, Nose-Hoover), H_2O barrier	100 K →200 K → 300 K	150 ps, 2 fs	Membrane headgroups restrained in z, protein heavy atoms: 10 kcal/mol*Å^2, gradual release
NVT (Nose-Hoover) equilibration	300 K	50 ps, 2 fs	Backbone + ligand (non-H): 5 kcal/mol*Å^2
NVT (MTK, Nose-Hoover), final unrestrained equilibration	300 K	50 ps, 2 fs	none
NPgT (MTK, Nose-Hoover), production	300 K	100 ns, 2 fs	none







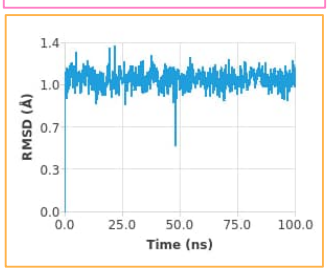


Figure S6: Molecular dynamics simulation system and details

WaterMap analysis (Schrödinger Suite 2022-4) indicated that compound **1** is accessible to the bulk solvent from the extracellular side of the receptor (top left). The all-atom simulation system (top right) utilized to get starting coordinates for water molecules in vicinity of **1** for docking grid generation was stable due to the time course of the simulation (bottom right). Simulation details are listed in bottom left. MRGPRX1 protein is shown in blue, MiniG protein in cyan, BAM8-22 in pink, compound **1** in orange, membrane in grey and water molecules in red. WaterMap hydration sites are shown as spheres ranging from green to red. Also, the RMSD plots in bottom right are color coded accordingly.

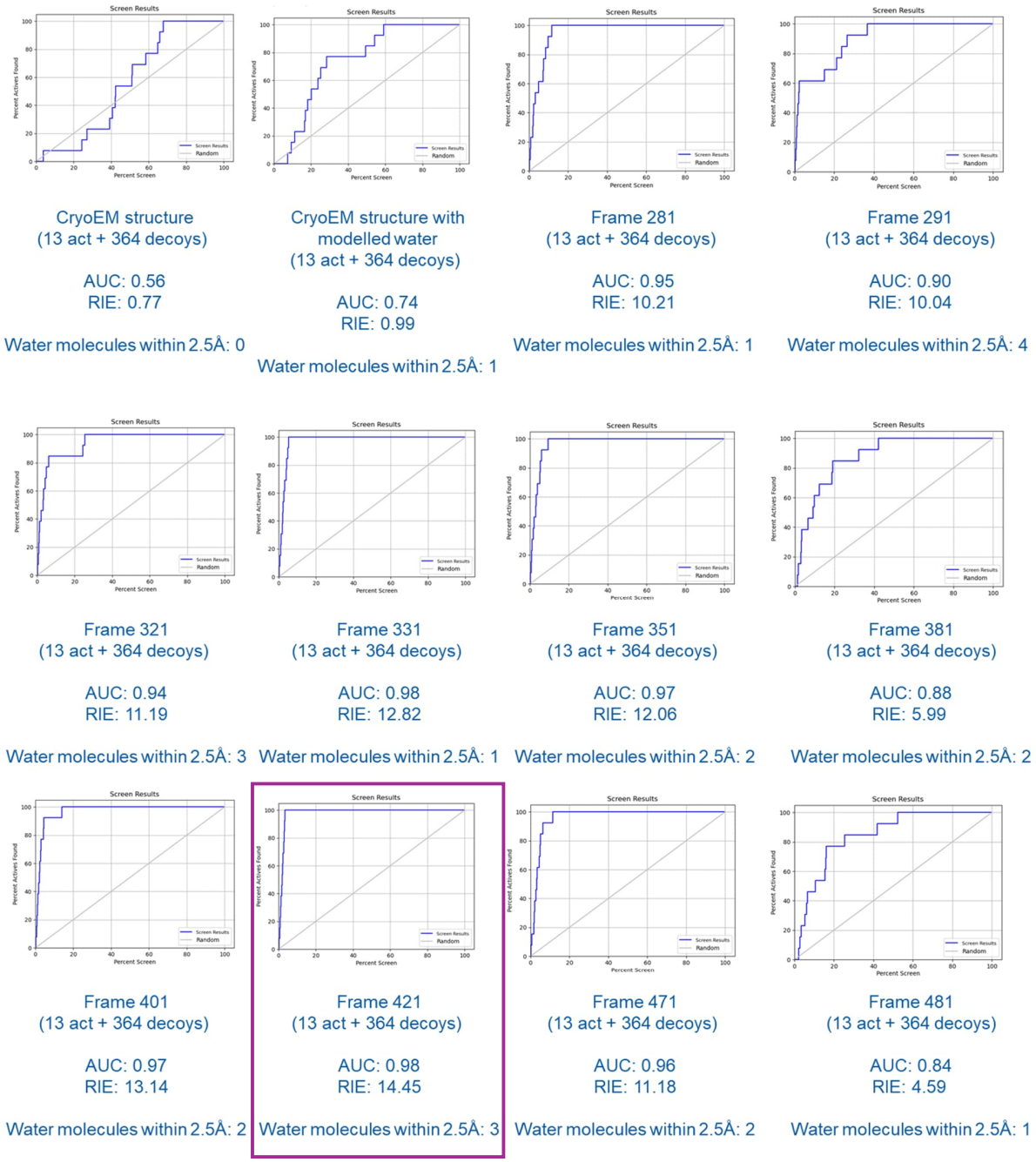


Figure S7: Enrichment plots of the studied docking grids

Altogether, 12 docking grids were studied for the enrichment of the known active compounds among the decoys. The first grid ("CryoEM structure") refers to the original MRGPRX1-

867 compound **1** complex by Liu et. al. with no added water molecules, whereas the second grid is the
868 same structure with a water molecule modelled based on one of the WaterMap hydration sites. The
869 rest of the grids are snapshots from the MD trajectory. Magenta rectangle indicates the best-
870 performing grid utilized for virtual screening.
871

Table S1. Data collection, refinement, and validation statistics

Table 1 – Data collection, refinement, and validation statistics				
	MRGPRX1-**9** (global refinement)	MRGPRX1-**9** (local refinement)	MRGPRX1-**8** (global refinement)	MRGPRX1-**8** (local refinement)
Data collection				
Microscope	Titan Krios G4		Glacios	
Voltage [kV]	300		200	
Camera	Falcon 4i		Falcon 4i	
Energy filter	Selectris X 10 eV slit width		Selectris X 10 eV slit width	
Collection mode	Counting		Counting	
Magnification	165,000 x		130,000 x	
Pixel size [Å/px]	0.731		0.87	
Exposure time [s]	2.1		4.6	
Electron exposure [e-/Å2]	50		50	
Defocus range [μm]	-0.7 to -2.0		-0.6 to -2.0	
No. of raw movies	12,805		6,297	
Data processing				
Processing software	Relion 5.0/cryoSPARC v4.7.0		Relion 5.0/cryoSPARC v4.7.0	
No. of movies used	12,678		4,106	
Initial particle images [no.]	6,768,637		2,691,949	
Final particle images [no.]	129,96	129,96	234,76	234,76
Symmetry imposed	C1	C1	C1	C1
Map resolution [Å]	2,33	2.63	2.63	2.87
FSC threshold	0.143	0.143	0.143	0.143
Map resolution range [Å]	2.0-5.6	2.3-4.8	2.3-5.3	2.5-4.7
Refinement and validation				
Initial model used [PDB-ID]	8DWG	8DWG	8DWG	8DWG
Model resolution [Å]	2.6	2.8	2.8	3.0
FSC threshold	0.5	0.5	0.5	0.5
Map sharpening B factor [Å2]	DeepEMhancer sharpened	DeepEMhancer sharpened	DeepEMhancer sharpened	DeepEMhancer sharpened
Model composition				
Non-hydrogen atoms	9007	2202	8947	2223
Protein residues	1129	269	1132	272
Ligands	2	2	2	2
B factors [Å2]				
Overall	87.55	67.53	98.49	82.24
R.m.s. deviations				
Bond lengths [Å]	0.005	0.005	0.004	0.005
Bond angles [°]	1.12	1.18	0.978	1.05
Validation				
MolProbity score	1.61	1.62	1.78	1.93
Clashscore	5.41	6.52	6.41	6.68
Poor rotamers [%]	1.13	0.82	1.64	2.85
Ramachandran plot				
Favored [%]	95.94	96.17	96.14	96.62
Allowed [%]	3.88	3.83	3.77	3.38
Disallowed [%]	0.18	0.00	0.09	0.00
	no flips	no flips	no flips	no flips

Table S2. Details for SPR data analysis

Software: Insight evaluation software (Cytiva)

Solvent correction: DMSO solvent correction was applied to all data

Subtraction: Reference surface subtraction and blank injection was applied to all curves.

Fit parameters:

Model type	Model name	Parameter	Fit	Initial value
Affinity	Steady state affinity	KD	Fit global	XMax
Affinity	Steady state affinity	Rmax	Fit global	Ymax
Affinity	Steady state affinity	offset	Fit global	Ymax/5
Kinetics	1:1 binding	ka	Fit global	1e5
Kinetics	1:1 binding	kd	Fit global	1e-3
Kinetics	1:1 binding	Rmax	Fit global	YMax
Kinetics	1:1 binding	tc	Fit global	1e8
Kinetics	1:1 binding	RI	Constant	0
Kinetics	1:1 binding	Drift	Constant	0

Supplementary methods

Abbreviation

HATU: O-(7-Azabenzotriazol-1-yl)-N,N,N′,N′-tetramethyluronium hexafluorophosphate

THF: Tetrahydrofuran

DIPEA: N,N-Diisopropylethylamine

DMF: N,N-Dimethylformamide

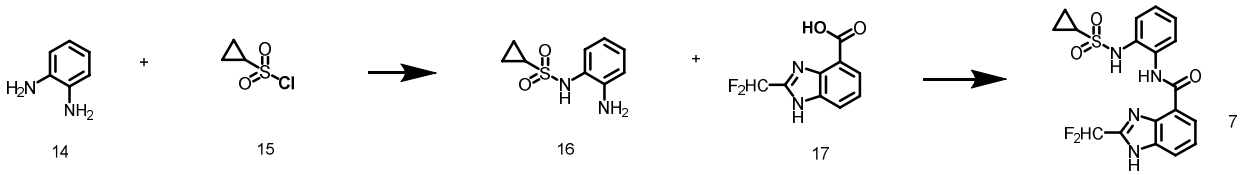
DMSO: Dimethyl Sulfoxide

DCM: Dichloromethane

RT: Room Temperature

HPLC: High-Performance Liquid Chromatography

Compound 7



Scheme 1. Synthesis of N-(2-(cyclopropanesulfonamido)phenyl)-2-(difluoromethyl)-1H-benzo[d]imidazole-4-carboxamide 7

Synthesis of N-(2-aminophenyl)cyclopropanesulfonamide 16

To a solution of benzene-1,2-diamine (50.0 mg, 1 Eq, 462 µmol) and pyridine (36.6 mg, 37.4 µL, 1 Eq, 462 µmol) in 1.4 ml THF at 0 °C was added cyclopropanesulfonyl chloride (65.0 mg, 1 Eq, 462 µmol) dropwise at 0°C. The reaction mixture was stirred at RT for 12h. The reaction was concentrated purified by flash silica gel chromatography (Biotage, 10g Sfär column, gradient with solvents hexane and ethyl acetate 0-100% @ 80 mL/min, λ-All) to yield 21mg (21%) of the target compound **16**.

LC-MS (acidic): Rt = 0.68 min; MS(ESIpos) m/z = 213.2 [M+H]+

1H NMR (400 MHz, DMSO-d6) δ ppm 0.79-0.85(m, 2 H) 0.86- 0.94 (m, 2 H) 5.07 (s, 2 H) 6.5 – 6.55 (m, 1 H) 6.69 – 6.73 (m, 1 H) 6.93 – 6.98 (m, 1 H) 7.05 – 7.09 (m, 1 H) 8.73 (s, 1 H)

Synthesis of N-(2-(cyclopropanesulfonamido)phenyl)-2-(difluoromethyl)-1H-benzo[d]imidazole-4-carboxamide 7

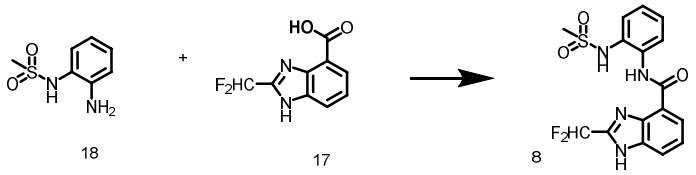
To a solution of 2-(difluoromethyl)-1H-benzo[d]imidazole-4-carboxylic acid (20.0 mg, 1 Eq, 94.3 µmol), HATU (71.7 mg, 2 Eq, 189 µmol) and DIPEA (48.7 mg, 4 Eq, 377 µmol) in 286 µL DMF at RT was added ORI003-0125 (21mg, 4 Eq, 104 µmol). The reaction mixture was stirred at RT for 12h. Water was added and extracted with EtOAc for 3 times. The combined organic phase was washed with brine and filtered via a water repellent filter circle (MN

617 WA) and evaporated to dryness. The residue was purified with HPLC to yield 8.8 mg (23%) of the target compound **7**.

LC-MS (HT-acidic): Rt = 1.04 min; MS(ESIpos) m/z = 407.2 [M+H]+

1H NMR (400 MHz, DMSO-d6) δ ppm 0.78 – 0.85 (m, 2 H) 0.9 – 0.98 (m, 2 H) 2.71 – 2.78 (m, 1 H) 7.13 – 7.2 (m, 1 H) 7.29 – 7.45 (m, 2 H) 7.45 – 7.5 (m, 1 H) 7.53 – 7.6 (m, 1 H) 7.86 – 7.91 (m, 1 H) 8.07 – 8.12 (m, 1 H) 8.6 – 8.65 (m, 1 H) 9.43 (s, 1 H) 12.2 (s, 1 H) 14.13 (s, 1 H)

Compound 8



Scheme 2. Synthesis of 2-(difluoromethyl)-N-(2-(methylsulfonamido)phenyl)-1H-benzo[d]imidazole-4-carboxamide 8

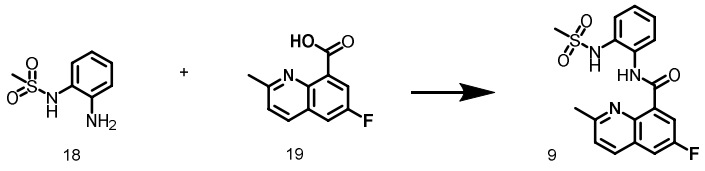
Synthesis of 2-(difluoromethyl)-N-(2-(methylsulfonamido)phenyl)-1H-benzo[d]imidazole-4-carboxamide 8

To a solution of 2-(difluoromethyl)-1H-benzo[d]imidazole-4-carboxylic acid (100 mg, 1 Eq, 471 µmol), HATU (358 mg, 2 Eq, 943 µmol) and DIPEA (244 mg, 4 Eq, 1.89 mmol) in 1.43 mL DMF at RT was added N-(2-aminophenyl)methanesulfonamide (123 mg, 1.4 Eq, 660 µmol). The reaction mixture was stirred at RT for 12h. Water was added and extracted with EtOAc for 3 times. The combined organic phase was washed with brine and filtered via a water repellent filter circle (MN 617 WA) and evaporated to dryness. The residue was purified with HPLC to yield 43 mg (24%) of the target compound **8**.

LC-MS (HT-acidic): Rt = 0.96 min; MS(ESIpos) m/z = 381.1 [M+H]+

1H NMR (400 MHz, DMSO-d6) δ ppm 3.05 (s, 3H) 7.15 – 7.21 (m, 1 H) 7.29 – 7.47 (m, 3 H) 7.54 – 7.6 (m, 1 H) 7.87 – 7.91 (m, 1 H) 8.07 – 8.12 (m, 1 H) 8.6 – 8.65 (m, 1 H) 9.42 (s, 1 H) 12.11 (s, 1 H) 14.14 (s, 1 H)

Compound 9



Scheme 3. Synthesis of 6-fluoro-2-methyl-N-(2-(methylsulfonamido)phenyl)quinoline-8-carboxamide 9

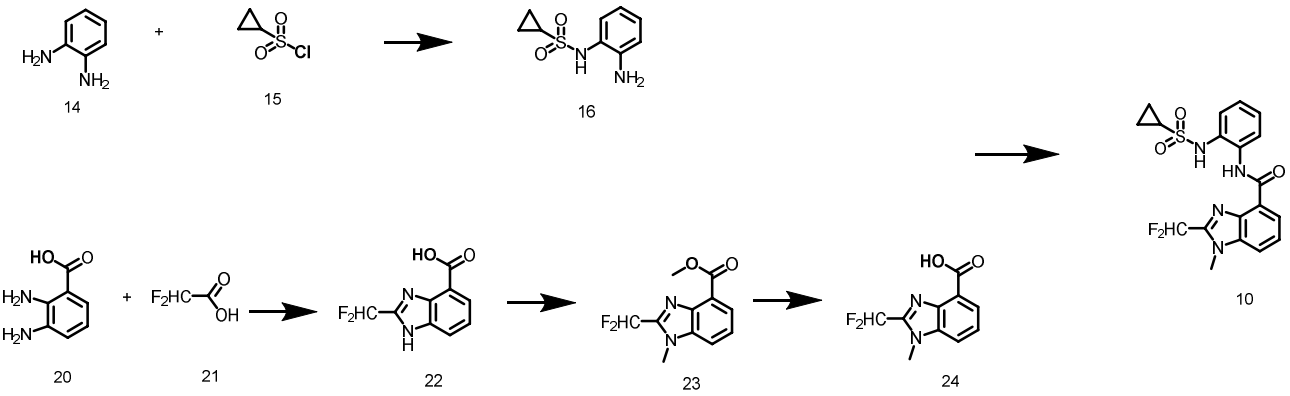
Synthesis of 6-fluoro-2-methyl-N-(2-(methylsulfonamido)phenyl)quinoline-8-carboxamide 9

To a solution of 6-fluoro-2-methylquinoline-8-carboxylic acid (50.0 mg, 1 Eq, 244 µmol), HATU (185 mg, 2 Eq, 487 µmol) and DIPEA (126 mg, 4 Eq, 975 µmol) in 738 µL DMF at RT was added N-(2-aminophenyl)methanesulfonamide (81.7 mg, 1.8 Eq, 439 µmol). The reaction mixture was stirred at RT for 12h. Water was added and extracted with EtOAc for 3 times. The combined organic phase was washed with brine and filtered via a water repellent filter circle (MN 617 WA) and evaporated to dryness. The residue was purified with HPLC to yield 38 mg (42%) of the target compound **9**.

LC-MS (HT-acidic): Rt = 1.14 min; MS(ESIpos) m/z = 374.16 [M+H]+

1H NMR (400 MHz, DMSO-d6) δ ppm 2.9 (s, 3H) 2.94 (s, 3H) 7.19 – 7.25 (m, 1 H) 7.35 – 7.43 (m, 2 H) 7.64 – 7.68 (m, 1 H) 8.06 – 8.11 (m, 1 H) 8.38 – 8.42 (m, 1 H) 8.42 – 8.46 (m, 1 H) 8.46 – 8.5 (m, 1 H) 9.31 (s, 1 H) 13.56 (s, 1 H)

Compound 10



Scheme 4. Synthesis of N-(2-(cyclopropanesulfonamido)phenyl)-2-(difluoromethyl)-1-methyl-1H-benzo[d]imidazole-4-carboxamide 10

Synthesis of N-(2-aminophenyl)cyclopropanesulfonamide 16

To a solution of benzene-1,2-diamine (250.0 mg, 1 Eq, 2.312 mmol) and pyridine (182.9 mg, 1 Eq, 2.312 mmol) in 2 ml THF was added cyclopropanesulfonyl chloride (390.0 mg, 1.2 Eq, 2.774 mmol) dropwise at RT. The reaction mixture was stirred at RT for 48h. The reaction was concentrated and used directly for the next step.

LC-MS (basic): Rt = 0.48 min; MS(ESIpos) m/z = 213.2 [M+H]+

Synthesis of 2-(difluoromethyl)-1H-benzo[d]imidazole-4-carboxylic acid 22

To a solution of 2,3-diaminobenzoic acid (1000 mg, 1 Eq, 6.572 mmol) in 49.29 mL 4 M HCl was added 2,2-difluoroacetic acid (2.525 g, 1.654 mL, 4 Eq, 26.29 mmol). The reaction was stirred at 105 °C for 15 hour. After cooling down to RT, 5mL water was added and basified with aqu. NH3. After filteration, the solution was neutralized with 10% H2SO4 to pH 5 and stirred at 0°C for 10min. The precipitate was filtered off to yield 1.16g (83.2%) of the target compound **22**.

LC-MS (acidic): Rt = 0.71 min; MS(ESIpos) m/z = 213.0 [M+H]+

1H NMR (400 MHz, DMSO-d6) δ ppm 7.09 – 7.38 (m, 1 H) 7.35 – 7.45 (m, 1 H) 7.89 – 7.96 (m, 1 H) 7.99 – 8.05 (m, 1 H) 13.14 (s, 1 H) 13.45 (s, 1 H)

Synthesis of methyl 2-(difluoromethyl)-1-methyl-1H-benzo[d]imidazole-4-carboxylate 23

To a solution of 2-(difluoromethyl)-1H-benzo[d]imidazole-4-carboxylic acid (100 mg, 1 Eq, 471 µmol) in 2 mL DMF was added NaH (23.6 mg, 60% Wt, 1.25 Eq, 589 µmol) at RT and stirred for 1 hour. Then MeI (140 mg, 61.9 µL, 2.1 Eq, 990 µmol) was added and stirred for 12 hour at RT. Another 0,5eq NaH and 0,5eq MeI were added and stirred for 3h at RT. Water was added and extracted with EtOAc for 3 times. The combined organic phase was washed with brine, filtered via a water repellent filter circle (MN 617 WA) and evaporated. The residue was purified by flash silica gel chromatography (Biotage, 10g Sfär column, gradient with solvents hexane and ethyl acetate 0-100% @ 80 mL/min, λ-All) to yield 90.6mg (80%) of the target compound **23**.

LC-MS (acidic): Rt = 0.89 min; MS(ESIpos) m/z = 241.1 [M+H]+

Synthesis of 2-(difluoromethyl)-1-methyl-1H-benzo[d]imidazole-4-carboxylic acid 24

To a solution of methyl 2-(difluoromethyl)-1-methyl-1H-benzo[d]imidazole-4-carboxylate (90 mg, 1 Eq, 0.37 mmol) in 2 mL MeOH was added 0.41 mL 1M NaOH (16 mg,1.1 Eq, 0.41 mmol) at RT and stirred for 12 hour. The reaction was cocentrated and treated with 10% H2SO4 till pH 5. Water was added and the mixture was extracted with EtOAc for 3 times. The combined organic phase was washed with brine, filtered via a water repellent filter circle (MN 617 WA) and evaporated. The Crude was used in the next step.

LC-MS (acidic): Rt = 0.83 min; MS(ESIpos) m/z = 227.0 [M+H]+

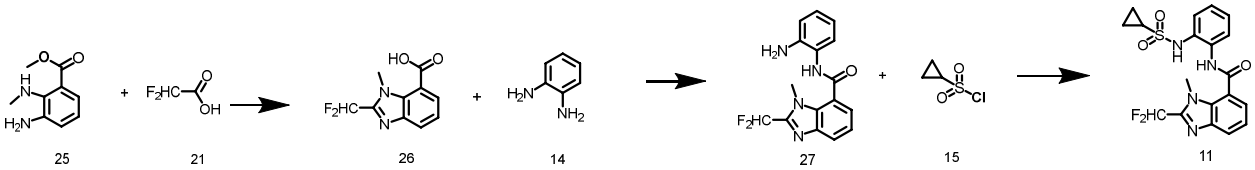
Synthesis of N-(2-(cyclopropanesulfonamido)phenyl)-2-(difluoromethyl)-1-methyl-1H-benzo[d]imidazole-4-carboxamide 10

To a solution of 2-(difluoromethyl)-1-methyl-1H-benzo[d]imidazole-4-carboxylic acid (40 mg, 1 Eq, 0.18 mmol), HATU (0.13 g, 2 Eq, 0.35 mmol) and DIPEA (91 mg, 0.12 mL, 4 Eq, 0.71 mmol) in 1mL DMF at RT was added N-(2-aminophenyl)cyclopropanesulfonamide (38 mg, 1 Eq, 0.18 mmol). The reaction mixture was stirred at RT for 12h. Water was added and extracted with EtOAc for 3 times. The combined organic phase was washed with brine and filtered via a water repellent filter circle (MN 617 WA) and evaporated to dryness. The residue was purified with HPLC to yield 5.2 mg (7%) of the target compound **10**.

LC-MS (HT-acidic): Rt = 1.13 min; MS(ESIpos) m/z = 421.1 [M+H]+

1H NMR (400 MHz, DMSO-d6) δ ppm 0.92 – 0.97 (m, 2 H) 0.82 – 0.87 (m, 2 H) 2.68 – 2.74 (m, 1 H) 4.09 (s, 3H) 7.14 – 7.18 (m, 1 H) 7.37 – 7.41 (m, 1 H) 7.47 – 7.5 (m, 1 H) 7.56 – 7.67 (m, 2 H) 8.04 – 8.07 (m, 1 H) 8.13 – 8.16 (m, 1 H) 8.65 – 8.68 (m, 1 H) 9.45 (s, 1 H) 12.17 (s, 1 H)

Compound 11



Scheme 5. Synthesis of N-(2-(cyclopropanesulfonamido)phenyl)-2-(difluoromethyl)-1-methyl-1H-benzo[d]imidazole-7-carboxamide 11

Synthesis of 2-(difluoromethyl)-1-methyl-1H-benzo[d]imidazole-7-carboxylic acid 26

To a solution of methyl 3-amino-2-(methylamino)benzoate (500 mg, 1 Eq, 2.77 mmol) in 21 mL 4 M HCl was added 2,2-difluoroacetic acid (1.07 g, 698 µL, 4 Eq, 11.1 mmol). The reaction was stirred at 105 °C for 15 hour. After cooling down to RT, 5mL water was added and basified with aqu. NH3. After filteration, the solution was neutralized with 10% H2SO4 to pH 5 and stirred at 0°C for 10min. The precipitate was filtered off to yield 648mg (100%) of the target compound **26**.

LC-MS (acidic): Rt = 0.73 min; MS(ESIpos) m/z = 227.1 [M+H]+

1H NMR (400 MHz, DMSO-d6) δ ppm 4.02 (s, 3 H) 7.3 – 7.6 (m, 2 H) 7.75 – 7.82 (m, 1 H) 7.92 – 7.98 (m, 1 H) 13.2 (s, 1 H)

Synthesis of N-(2-aminophenyl)-2-(difluoromethyl)-1-methyl-1H-benzo[d]imidazole-7-carboxamide 27

To a solution of 2-(difluoromethyl)-1-methyl-1H-benzo[d]imidazole-7-carboxylic acid (75 mg, 1 Eq, 0.33 mmol), HATU(0.25 g, 2 Eq, 0.66 mmol) and DIPEA (0.17 g, 0.23 mL, 4 Eq, 1.3 mmol) in 1mL DMF at RT was added benzene-1,2-diamine (36 mg, 1 Eq, 0.33 mmol). The reaction mixture was stirred at RT for 12h. The reaction was concentrated purified by flash silica gel chromatography (Biotage, 10g Sfär column, gradient with solvents hexane and ethyl acetate 0-100% @ 80 mL/min, λ-All) to yield 61mg (61%) of the target compound **27**.

LC-MS (acidic): Rt = 0.84min; MS(ESIpos) m/z = 317.4 [M+H]+

1H NMR (400 MHz, DMSO-d6) δ ppm 3.94 (s, 3 H) 5.04 (s, 2 H) 6.58 – 6.64 (m, 1 H) 6.76 – 6.81 (m, 1 H) 6.96 – 7.01 (m, 1 H) 7.29 – 7.61 (m, 3 H) 7.66 – 7.71 (m, 1 H)7.88 – 7.93 (m, 1 H) 9.86 (s, 1 H)

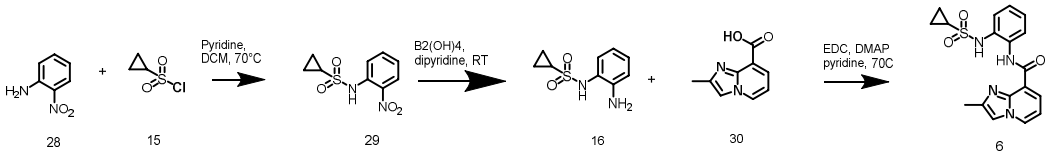
Synthesis of N-(2-(cyclopropanesulfonamido)phenyl)-2-(difluoromethyl)-1-methyl-1H-benzo[d]imidazole-7-carboxamide 11

To a solution of N-(2-aminophenyl)-2-(difluoromethyl)-1-methyl-1H-benzo[d]imidazole-7-carboxamide (30 mg, 1 Eq, 95 µmol) and pyridine (7.5 mg, 7.7 µL, 1 Eq, 95 µmol) in 2 ml THF was added cyclopropanesulfonyl chloride (16 mg,1.2 Eq, 0.11 mmol) at RT. The reaction mixture was stirred at RT for 12h. Another 1eq. of cyclopropanesulfonyl chloride (16 mg, 10 µL, 1.2 Eq, 0.11 mmol) and 1eq. of pyridine (7.5 mg, 7.7 µL, 1 Eq, 95 µmol) were added and stirred at RT for 12h. The reaction was concentrated and purified with HPLC to yield 4.7 mg (12%) of the target compound **11**.

LC-MS (basic): Rt = 0.65 min; MS(ESIpos) m/z = 421.3 [M+H]+

1H NMR (400 MHz, DMSO-d6) δ ppm 0.81 – 0.88 (m, 2 H) 0.91 – 0.96 (m, 2 H) 2.55 – 2.72 (m, 1 H) 3.93 (s, 3 H) 7.23 – 7.37 (m, 2 H) 7.4 – 7.62 (m, 3 H) 7.7 – 7.75 (m, 1 H) 7.86 – 7.92 (m, 1 H) 7.93 – 7.99 (m, 1 H) 9.15 (s, 1 H) 10.02 (s, 1 H)

Compound 6



Scheme 6. Synthesis of N-(2-(cyclopropanesulfonamido)phenyl)-2-methylimidazo[1,2-a]pyridine-8-carboxamide 6

Synthesis of N-(2-nitrophenyl)-cyclopropanesulfonamide 29

To a solution of 2-nitroaniline (2.000 g, 1 Eq, 14.48 mmol) in DCM (20.000 mL) was added pyridine (22.91 g, 23.4 mL, 20 Eq, 289.6 mmol) and cyclopropanesulfonyl chloride (3.053 g, 1.5 Eq, 21.72 mmol). The reaction was stirred at 70 °C for 48 hours. After cooling down to RT, the reaction mass was diluted with diethyl acetate and water, and extracted with diethyl acetate. The organic layer was concentrated and purified by flash silica gel chromatography to yield 1,55g (43%) of the target compound **29**.

LC-MS: Rt = 1,90 min; MS(ESIneg) m/z = 241.0 [M-H]+

1H NMR (400 MHz, DMSO-d6) δ ppm 0.90 – 0.95 (m, 2 H) 0.95-1.00 (m, 2 H) 2.72– 2.79 (m, 1H) 7.40 – 7.45 (m, 1 H) 7.61 – 7.64 (m, 1 H) 7.70-7.75 (m, 1 H) 7.98 – 8.01 (m, 1 H) 9.83 (s, 1 H)

Synthesis of N-(2-aminophenyl)-cyclopropanesulfonamide 16

To a solution of N-(2-nitrophenyl)cyclopropanesulfonamide (1.500 g, 1 Eq, 6.192 mmol) in DMF (20.000 mL) was added Hypodiboric acid (1.388 g, 2.5 Eq, 15.48 mmol) and gamma,gamma'-Dipyridyl (48.36 mg, 0.05 Eq, 309.6 µmol) .The reaction was stirred at 25 °C for 1 hour. The reaction mass was diluted with diethyl acetate and water, and extracted with diethyl acetate. The organic layer was concentrated and purified by flash silica gel chromatography to yield 850 mg (63%) of the target compound **16**.

LC-MS: Rt = 1,34 min; MS(ESIpos) m/z = 213.0 [M+H]+

1H NMR (400 MHz, DMSO-d6) δ ppm 0.81 – 0.86 (m, 2 H) 0.87-0.93 (m, 2 H) 2.53 – 2.58 (m, 1H) 5.06 (s, 2 H) 6.50 – 6.55 (m, 1 H) 6.70 – 6.72 (m, 1 H) 6.94-6.98 (m, 1 H) 7.06 – 7.09 (m, 1 H) 8.71 (s, 1 H)

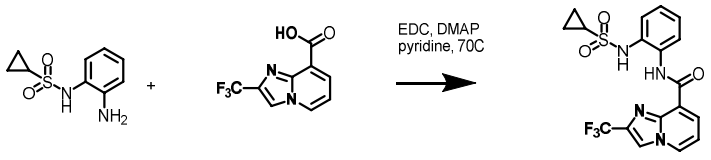
Synthesis of N-(2-(cyclopropanesulfonamido)phenyl)-2-methylimidazo[1,2-a]pyridine-8-carboxamide 6

To a solution of N-(2-aminophenyl)cyclopropanesulfonamide (100.00 mg, 1 Eq, 471.10 µmol) in Pyridine (2.000 mL) was added 2-methylimidazo[1,2-a]pyridine-8-carboxylic acid (99.592 mg, 1.2 Eq, 565.32 µmol) and DMAP (28.777 mg, 0.5 Eq, 235.55 µmol). The reaction was stirred at 70 °C for 1 hour. After cooling down to RT, the reaction mass was diluted with diethyl acetate and water, and extracted with diethyl acetate. The organic layer was concentrated and purified by flash silica gel chromatography to yield 21mg (12%) of the target compound **6**.

LC-MS: Rt = 5,58 min; MS(ESIpos) m/z = 371.3 [M+H]+

1H NMR (400 MHz, DMSO-d6) δ ppm 0.71 – 0.75(m, 2 H) 0.79-0.88 (m, 2 H) 2.81 – 2.87 (m, 1H) 7.06 – 7.10 (m, 1 H) 7.13 – 7.18 (m, 1 H) 7.32 – 7.36 (m, 1 H) 7.43-7.45 (m, 1 H) 7.89-7.90 (m, 1 H) 8.06-8.08 (m, 1 H) 8.49-8.51 (m, 1 H) 8.72-8.75 (m, 1 H) 9.33 (s, 1 H) 12.68 (s, 1 H)

Compound 3



16 31 3

Scheme 7. Synthesis of N-(2-(cyclopropanesulfonamido)phenyl)-2-(trifluoromethyl)imidazo[1,2-a]pyridine-8-carboxamide 3

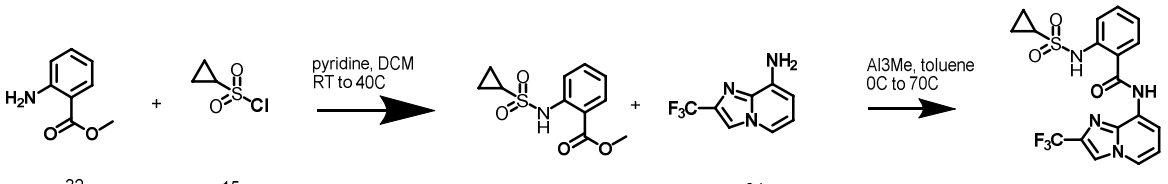
Synthesis of N-(2-(cyclopropanesulfonamido)phenyl)-2-(trifluoromethyl)imidazo[1,2-a]pyridine-8-carboxamide 3

To a solution of N-(2-aminophenyl)cyclopropanesulfonamide (100.00 mg, 1 Eq, 471.10 µmol) in Pyridine (2.000 mL) was added EDC (180.62 mg, 2 Eq, 942.20 µmol), 2-(trifluoromethyl)imidazo[1,2-a]pyridine-8-carboxylic acid (130.11 mg, 1.2 Eq, 565.32 µmol) and DMAP (28.777 mg, 0.5 Eq, 235.55 µmol). The reaction was stirred at 70 °C for 1 hour. After cooling down to RT, the reaction mass was diluted with diethyl acetate and water, and extracted with diethyl acetate. The organic layer was concentrated and purified by reverse phase column chromatography to yield 95mg (47%) of the target compound **3** as a trifluoroacetic salt.

LC-MS: Rt = 5,88 min; MS(ESIpos) m/z = 425.3 [M+H]+

1H NMR (400 MHz, DMSO-d6) δ ppm 0.73 – 0.78(m, 2 H) 0.78-0.88 (m, 2 H) 2.62 – 2.69 (m, 1H) 7.19 – 7.24 (m, 1 H) 7.31 – 7.38 (m, 2 H) 7.38 – 7.44 (m, 1 H) 8.20-8.22 (m, 1 H) 8.29-8.31 (m, 1 H) 8.77-8.78 (m, 1 H) 8.85-8.87 (m, 1 H) 9.29 (s, 1 H) 11.58 (s, 1 H)

Compound 4



32 15 33 34 4

Scheme 8. Synthesis of 2-(cyclopropanesulfonamido)-N-(2-(trifluoromethyl)imidazo[1,2-a]pyridin-8-yl)benzamide 4

Synthesis of methyl 2-(cyclopropanesulfonamido)benzoate 33

To a solution of methyl 2-aminobenzoate (1.000 g, 1 Eq, 6.615 mmol) in DCM (20.000 mL) was added pyridine (10.47 g, 10.7 mL, 20 Eq, 132.3 mmol) and cyclopropanesulfonyl chloride (1.860 g, 2.0 Eq, 13.23 mmol) at RT. The reaction was stirred at 40 °C for 12 hours. After cooling down to RT, the reaction mass was diluted in water and extracted with diethyl acetate. The organic layer was washed with NaCl solution and dried over Na2So4. The crude was concentrated under and purified by column chromatography using EtOAc and heptane as eluent to yield 600mg (34%) of the target compound **33**.

LC-MS: Rt = 2,08 min; MS(ESIpos) m/z = 256.06 [M+H]+

1H NMR (400 MHz, DMSO-d6) δ ppm 0.97 – 0.99 (m, 4 H) 2.79 – 2.85 (m, 1H) 3.90 (s, 3 H) 7.22 – 7.26 (m, 1 H) 7.64 – 7.68 (m, 2 H) 7.96 – 7.98 (m, 1 H) 10.11 (s, 1 H)

Synthesis of 2-(cyclopropanesulfonamido)-N-(2-(trifluoromethyl)imidazo[1,2-a]pyridin-8-yl)benzamide 4

To a stirred solution of 2-(trifluoromethyl)imidazo[1,2-a]pyridin-8-amine (118.19 mg, 1.0 Eq, 587.57 µmol) in Toluene (5.000 mL), trimethylaluminum (127.1 mg, 881.35 µL, 2.000 molar, 3 Eq, 1.7627 mmol) and methyl 2-(cyclopropanesulfonamido)benzoate (150.00 mg, 1 Eq, 587.57 µmol) were added at 0°C. The reaction was stirred at 70 °C for 16 hours. After cooling down to RT, the reaction mass was diluted with water and extracted with diethyl acetate. The organic layer dried over sodium sulfate, concentrated under reduced pressure and purified by reverse preparative HPLC to yield 48mg (19%) of the target compound **4**.

LC-MS: Rt = 6,01 min; MS(ESIpos) m/z = 425.3 [M+H]+

1H NMR (400 MHz, DMSO-d6) δ ppm 0.88 – 0.94 (m, 4 H) 2.71 – 2.77 (m, 1H) 7.10 – 7.14 (m, 1 H) 7.39 – 7.42 (m, 1 H) 7.55 – 7.65 (m, 1 H) 7.99 – 8.04 (m, 2 H) 8.42 – 8.45 (m, 1 H) 8.62 (s, 1 H) 10.17 (s, 1 H) 10.52 (s, 1 H)

References

1 Lorente, J. S. *et al.* GPCR drug discovery: new agents, targets and indications. *Nat Rev Drug Discov* **24**, 458-479 (2025). https://doi.org/10.1038/s41573-025-01139-y

2 Al Hamwi, G. *et al.* MAS-related G protein-coupled receptors X (MRGPRX): Orphan GPCRs with potential as targets for future drugs. *Pharmacol Ther* **238**, 108259 (2022). https://doi.org/10.1016/j.pharmthera.2022.108259

3 Lembo, P. M. *et al.* Proenkephalin A gene products activate a new family of sensory neuron--specific GPCRs. *Nat Neurosci* **5**, 201-209 (2002). https://doi.org/10.1038/nn815

4 Sikand, P., Dong, X. & LaMotte, R. H. BAM8-22 peptide produces itch and nociceptive sensations in humans independent of histamine release. *J Neurosci* **31**, 7563-7567 (2011). https://doi.org/10.1523/JNEUROSCI.1192-11.2011

5 Li, Z. *et al.* Targeting human Mas-related G protein-coupled receptor X1 to inhibit persistent pain. *Proc Natl Acad Sci U S A* **114**, E1996-E2005 (2017). https://doi.org/10.1073/pnas.1615255114

6 Uniyal, A. *et al.* An orally bioavailable MrgprX1-positive allosteric modulator alleviates certain neuropathic pain-related behaviors in humanized mice. *Sci Transl Med* **17**, eadw9446 (2025). https://doi.org/10.1126/scitranslmed.adw9446

7 Guo, L. *et al.* Ligand recognition and G protein coupling of the human itch receptor MRGPRX1. *Nat Commun* **14**, 5004 (2023). https://doi.org/10.1038/s41467-023-40705-z

8 Wen, W. *et al.* Discovery and characterization of 2-(cyclopropanesulfonamido)-N-(2-ethoxyphenyl)benzamide, ML382: a potent and selective positive allosteric modulator of MrgX1. *ChemMedChem* **10**, 57-61 (2015). https://doi.org/10.1002/cmdc.201402277

9 McMillan, H. *et al.* Endogenous Mas-related G-protein-coupled receptor X1 activates and sensitizes TRPA1 in a human model of peripheral nerves. *FASEB J* **35**, e21492 (2021). https://doi.org/10.1096/fj.202001667RR

10 Li, X. *et al.* Tick peptides evoke itch by activating MrgprC11/MRGPRX1 to sensitize TRPV1 in pruriceptors. *J Allergy Clin Immunol* **147**, 2236-2248 e2216 (2021). https://doi.org/10.1016/j.jaci.2020.12.626

11 Tseng, P. Y., Zheng, Q., Li, Z. & Dong, X. MrgprX1 Mediates Neuronal Excitability and Itch Through Tetrodotoxin-Resistant Sodium Channels. *Itch (Phila)* **4** (2019). https://doi.org/10.1097/itx.0000000000000028

12 Liu, Y. *et al.* Ligand recognition and allosteric modulation of the human MRGPRX1 receptor. *Nat Chem Biol* **19**, 416-422 (2023). https://doi.org/10.1038/s41589-022-01173-6

13 Nehme, R. *et al.* Mini-G proteins: Novel tools for studying GPCRs in their active conformation. *PLoS One* **12**, e0175642 (2017). https://doi.org/10.1371/journal.pone.0175642

14 Sharma, S. *et al.* Synthesis and Biological Characterization of a Series of 2-Sulfonamidebenzamides as Allosteric Modulators of MrgX1. *ACS Med Chem Lett* **13**, 841-847 (2022). https://doi.org/10.1021/acsmedchemlett.2c00100

15 Kalliokoski, T. Machine Learning Boosted Docking (HASTEN): An Open-source Tool To Accelerate Structure-based Virtual Screening Campaigns. *Mol Inform* **40**, e2100089 (2021). https://doi.org/10.1002/minf.202100089

16 Chen, H. & Ikeda, S. R. Modulation of ion channels and synaptic transmission by a human sensory neuron-specific G-protein-coupled receptor, SNSR4/mrgX1, heterologously expressed in cultured rat neurons. *J Neurosci* **24**, 5044-5053 (2004). https://doi.org/10.1523/JNEUROSCI.0990-04.2004

17 Maeda, S. *et al.* Development of an antibody fragment that stabilizes GPCR/G-protein complexes. *Nat Commun* **9**, 3712 (2018). https://doi.org/10.1038/s41467-018-06002-w

18 Garcia-Nafria, J. & Tate, C. G. Structure determination of GPCRs: cryo-EM compared with X-ray crystallography. *Biochem Soc Trans* **49**, 2345-2355 (2021). https://doi.org/10.1042/BST20210431

19 Liang, Y. L. *et al.* Phase-plate cryo-EM structure of a class B GPCR-G-protein complex. *Nature* **546**, 118-123 (2017). https://doi.org/10.1038/nature22327

20 Gan, B. *et al.* Mechanism of agonist-induced activation of the human itch receptor MRGPRX1. *PLoS Biol* **21**, e3001975 (2023). https://doi.org/10.1371/journal.pbio.3001975

21 Shen, S. *et al.* Allosteric modulation of G protein-coupled receptor signaling. *Front Endocrinol (Lausanne)* **14**, 1137604 (2023). https://doi.org/10.3389/fendo.2023.1137604

22 Lomize, M. A., Pogozheva, I. D., Joo, H., Mosberg, H. I. & Lomize, A. L. OPM database and PPM web server: resources for positioning of proteins in membranes. *Nucleic Acids Res* **40**, D370-376 (2012). https://doi.org/10.1093/nar/gkr703

23 Mastronarde, D. N. Automated electron microscope tomography using robust prediction of specimen movements. *J Struct Biol* **152**, 36-51 (2005). https://doi.org/10.1016/j.jsb.2005.07.007

24 Scheres, S. H. RELION: implementation of a Bayesian approach to cryo-EM structure determination. *J Struct Biol* **180**, 519-530 (2012). https://doi.org/10.1016/j.jsb.2012.09.006

25 Rohou, A. & Grigorieff, N. CTFFIND4: Fast and accurate defocus estimation from electron micrographs. *J Struct Biol* **192**, 216-221 (2015). https://doi.org/10.1016/j.jsb.2015.08.008

26 Bepler, T. *et al.* Positive-unlabeled convolutional neural networks for particle picking in cryo-electron micrographs. *Nat Methods* **16**, 1153-1160 (2019). https://doi.org/10.1038/s41592-019-0575-8

27 Punjani, A., Rubinstein, J. L., Fleet, D. J. & Brubaker, M. A. cryoSPARC: algorithms for rapid unsupervised cryo-EM structure determination. *Nat Methods* **14**, 290-296 (2017). https://doi.org/10.1038/nmeth.4169

28 Sanchez-Garcia, R. *et al.* DeepEMhancer: a deep learning solution for cryo-EM volume post-processing. *Commun Biol* **4**, 874 (2021). https://doi.org/10.1038/s42003-021-02399-1

29 Emsley, P. & Cowtan, K. Coot: model-building tools for molecular graphics. *Acta Crystallogr D Biol Crystallogr* **60**, 2126-2132 (2004). https://doi.org/10.1107/S0907444904019158

30 Murshudov, G. N. *et al.* REFMAC5 for the refinement of macromolecular crystal structures. *Acta Crystallogr D Biol Crystallogr* **67**, 355-367 (2011). https://doi.org/10.1107/S0907444911001314

31 Yamashita, K., Wojdyr, M., Long, F., Nicholls, R. A. & Murshudov, G. N. GEMMI and Servalcat restrain REFMAC5. *Acta Crystallogr D Struct Biol* **79**, 368-373 (2023). https://doi.org/10.1107/S2059798323002413

32 Chen, V. B. *et al.* MolProbity: all-atom structure validation for macromolecular crystallography. *Acta Crystallogr D Biol Crystallogr* **66**, 12-21 (2010). https://doi.org/10.1107/S0907444909042073

Supplementary Files

This is a list of supplementary files associated with this preprint. Click to download.

- TurkuMetsanenMDframes.zip
- MRGPRX1compound8.zip
- MRGPRX1compound9.zip
- TurkuMetsanennrreportingsummary.pdf
- MolecularDynamicsSimulationsChecklistTurkuMetsanenetal2026.docx